Coordinated stimulation of axon regenerative and neurodegenerative transcriptional programs by ATF4 following optic nerve injury

Preethi Somasundaram[1], Madeline M. Farley[1], Melissa A. Rudy[1,3], Katya Sigal[3], Andoni I. Asencor[3], David G. Stefanoff[1], Malay Shah[1], Puneetha Goli[1], Jenny Heo[1], Shufang Wang[1], Nicholas M. Tran[2], and Trent A. Watkins[1,3,4]

Departments of Neurosurgery[1] and Mol. & Human Genetics[2], Baylor College of Medicine, 1 Baylor Plaza, Houston, Texas 77030, USA

[3]Division of Neuroimmunology and Glial Biology, Department of Neurology, University of California-San Francisco, San Francisco, CA 94158

[4]Lead contact

Correspondence: Trent.Watkins@ucsf.edu

Keywords: Neurodegeneration; Axon regeneration; Stress signaling; Transcription factor

Abstract

Stress signaling is important for determining the fates of neurons following axonal insults. Previously we showed that the stress-responsive kinase PERK contributes to injury-induced neurodegeneration (Larhammar et al., 2017). Here we show that PERK acts primarily through Activating Transcription Factor-4 (ATF4) to stimulate not only pro-apoptotic but also pro-regenerative responses following optic nerve damage. Using conditional knockout mice, we find an extensive PERK/ATF4-dependent transcriptional response that includes canonical ATF4 target genes and modest contributions by C/EBP Homologous Protein (CHOP). Overlap with c-Jun-dependent transcription suggests interplay with a parallel stress pathway that orchestrates regenerative and apoptotic responses. Accordingly, neuronal knockout of ATF4 recapitulates the neuroprotection afforded by PERK deficiency, and PERK or ATF4 knockout impairs optic axon regeneration enabled by disrupting the tumor suppressor PTEN. These findings reveal an integral role for PERK/ATF4 in coordinating neurodegenerative and regenerative responses to CNS axon injury.

Introduction

Experiments using conditional knockout mice have revealed a critical role for stress signaling-mediated transcriptional responses in determining the fates of neurons after axon injury. Prominent among these, neuronal knockout of the stress-responsive Dual leucine-zipper kinase (DLK) suppresses the stimulation by injury of transcription factors of the bZIP family, including c-Jun and the Activating transcription factor-3 (ATF3), that substantially alter the transcriptomes of distressed neurons (Asghari Adib et al., 2018; Farley and Watkins, 2018; Le Pichon et al., 2017; Tran et al., 2019; Welsbie et al., 2017, 2013). As is common in cellular stress signaling, this injury-induced MAP kinase (MAPK) signaling cascade couples the activation of transcriptional programs that prime damaged neurons for repair with those that prime those same neurons for apoptosis, the latter a feature that may facilitate the elimination of irreparable cells (Watkins et al., 2013).

These and other essential insights have been enabled by mouse optic nerve crush, an exceptionally tractable model for CNS axon injury that has been valuable for understanding axonopathy-driven CNS neurodegeneration, particularly glaucoma, and the neuron-intrinsic and extrinsic factors that limit CNS axon regeneration (Lindborg et al., 2021; Tran et al., 2019; Vidal-Sanz et al., 2017). Following crush injury, axotomized retinal ganglion cells (RGCs) face both intrinsic and environmental barriers to axon regeneration, and the pro-apoptotic aspects of this response ultimately result in extensive RGC neurodegeneration over subsequent weeks (Syc-Mazurek et al., 2017a; Watkins et al., 2013; Welsbie et al., 2013, 2017). Though neuronal knockout of DLK, c-Jun, or ATF3 each confer considerable RGC neuroprotection, disrupting these also limits the upregulation of regeneration-associated genes (RAGs) and the success of regenerative interventions, such as knockout of the tumor suppressor PTEN, that offer promise for enabling CNS repair (Jacobi et al., 2022; Watkins et al., 2013). Devising strategies to suppress neuronal loss without restricting intrinsic programs for repair will therefore require improving our understanding of which pathways and effectors within the injury response control axon regenerative and neurodegenerative programs and how these overlap (Patel et al., 2020).

Of particular interest is deciphering the contributions of the Integrated Stress Response (ISR). The ISR, activated in parallel to c-Jun as part of the DLK signaling cascade (Larhammar et al., 2017), results in the suppression of general translation but enhanced transcription and translation of select mRNAs, including *Atf4*, encoding the Activating transcription factor-4 (ATF4), and *Ddit3*, encoding the C/EBP homologous protein (CHOP) (Pitale et al., 2017). Both ATF4 and CHOP have the potential to regulate transcription of ATF3 and/or heterodimerize with c-Jun, ATF3, other transcription factors of the C/EBP family, or each other, raising the possibility of crosstalk between the ISR and MAPK arms of the DLK response (Pakos-Zebrucka et al., 2016). Genetic disruption of ISR activation or of neuronal *Eif2ak3*, the gene encoding the ISR-activating kinase PERK, confers significant but incomplete RGC neuroprotection after optic nerve crush (Larhammar et al., 2017; Yang et al., 2016). These findings demonstrate that the neuronal ISR represents a functional component of the intrinsic neurodegenerative response but have provided limited mechanistic insight.

Recent studies emphasize the importance of defining the downstream effectors of the ISR, their relationships to c-Jun, and their impacts on RGC axon regenerative potential. Based on CRISPR screening, RNA-seq, and ATAC-seq, Tian *et al.* (2022) proposed that ATF4 serves, along with C/EBPγ, as a critical component of a core neurodegenerative program, with CHOP and ATF3 together mediating a second core program (Tian et al., 2022). Injured RGCs expressing *Cas9* and a gRNA pool targeting ATF4 exhibited improved survival and modulation of genes primarily associated with intrinsic neuronal stressors (*e.g.*, DNA damage response, autophagy, and the NAD/p53 pathway) distinct from canonical ATF4 target genes for adapting to amino acid deprivation, endoplasmic reticulum stress, and other ISR-activating insults. Additive to this, partial neuroprotection could also be achieved by gRNA pools targeting either Ddit3/CHOP or ATF3, either of which resulted in extensive, highly overlapping, transcriptional consequences related to cytokines and innate immunity (Tian et al., 2024, 2022). Importantly, a companion report shows that, of these same gRNA pools, only targeting ATF3 reduced RGC axon regeneration enabled

by knockout of the tumor suppressor PTEN (Jacobi et al., 2022). Conditional knockout of ATF4 and CHOP has been reported to provide more neuroprotection than either alone, despite knockout of either appearing in that study to be sufficient to deplete the mRNA for both (Fang et al., 2023). Together, these findings led to the proposal that ATF4 and CHOP function in parallel neurodegenerative programs and, unlike ATF3 and c-Jun, do so without influencing RGC axon regenerative potential.

Other reports, however, seem to be inconsistent with these non-canonical roles for ATF4 and CHOP. The DLK-mediated stress response includes ISR-dependent upregulation of *Chac1*, *Ddit3*, and other target genes consistent with a typical ATF4-mediated transcriptional program, inclusive of CHOP activation (Larhammar et al., 2017). In addition, the proposed role of CHOP as a principal neuron-intrinsic effector of the response to optic nerve injury appears to be incongruent with the mild impact of germline *Ddit3*/CHOP knockout on that response. RNA-seq of retinae from these mice uncovered few injury-induced transcripts that were significantly suppressed relative to the extensive impact of neural knockout of c-Jun (Syc-Mazurek et al., 2022). Though these CHOP-null mice reproducibly exhibit partial RGC neuroprotection (Hu et al., 2012; Syc-Mazurek et al., 2017b), the modest influence of CHOP deficiency on the transcriptome suggests the need for further evaluation of whether its primary role in regulating RGC survival is neuron-autonomous, as it may also reflect developmental effects or influences on other cell types, perhaps outside of the retina.

Here we use previously validated conditional knockout (cKO) mice lines to directly address these and other questions raised by germline knockout and CRISPR studies. We find that a canonical ATF4 response functions as the principal mediator of a PERK-activated response that broadly contributes to both RGC apoptosis and axon regenerative potential. Unexpectedly, neuronal CHOP, long considered to be a primary neuron-intrinsic effector of the ISR in injured RGCs, plays a relatively modest role within these PERK/ATF4-stimulated programs. These findings reveal an integral role for PERK-stimulated ATF4 in the response to optic axon damage,

serving to link neurodegenerative and axon regenerative transcriptional programs that determine the fates of distressed neurons.

Results

Neuronal ATF4 knockout mimics the neuroprotection provided by PERK deletion

Deletion of neuronal PERK, a key mediator of the ISR after optic nerve crush, provides significant, though incomplete, neuroprotection to RGCs (Larhammar et al., 2017). To determine how the ISR effectors ATF4 and CHOP contribute to neurodegeneration, we evaluated the survival of RGCs in cKO mice using immunohistochemistry for the pan-RGC marker RBPMS. We used high-titer intravitreal injection of AAV serotype 2 (AAV2) harboring the human synapsin-1 promoter (*hSyn1*), resulting in widespread Cre activity throughout neurons of the ganglion cell layer and inner nuclear layer of the retina (**Supplemental Figure S1A-B**). We confirmed the expected loss of *Atf4* transcript in ATF4 cKO mice and *Ddit3*/CHOP transcript in CHOP cKO mice by RNAScope (**Supplemental Figure S1C-D**). Evaluation of neuronal survival two weeks after optic nerve crush revealed that targeting ATF4, but, surprisingly, not CHOP, confers significant neuroprotection of RBPMS-expressing RGCs (**Figure 1A**). We next compared the neuroprotection measured by this method with that determined using phospho-c-Jun as a robust, easily quantifiable nuclear marker of injured RGCs, finding similar improvements to RGC survival upon ATF4 knockout using either method (**Figure 1B**). To determine if CHOP disruption might augment the neuroprotection conferred by ATF4 disruption, we generated ATF4/CHOP double conditional knockout (dcKO) mice. However, these mice did not exhibit significantly greater RGC survival than ATF4 cKO mice (**Figure 1C**). Finally, we directly compared the effects of PERK knockout and ATF4 knockout, finding disruption of ATF4 is sufficient to afford a similar degree of neuroprotection to that of PERK (**Figure 1D**). Together with previous findings that ATF4 activation is DLK- and PERK-dependent (Larhammar et al., 2017), these results suggest that ATF4 serves as the primary mediator of the pro-apoptotic effects of the ISR after optic nerve crush.

Neuronal PERK mediates an extensive contribution to the injury response primarily through ATF4

The equivalent neuroprotection afforded by knockout of PERK and ATF4 raises the possibility that ATF4 may be the principal neuron-autonomous mediator of ISR-activated transcription influencing RGC survival. To better understand the contributions of PERK and its effectors to the transcriptional response, we performed expression profiling of retina by RNA-seq three days after optic nerve crush in wildtype mice and three cKO lines: *Eif2ak3* cKO to disrupt PERK, *Ddit3* cKO to disrupt CHOP, and *Atf4* cKO to disrupt ATF4 (**Table S1**).

We began by determining the contribution of PERK and its effectors to the transcriptional injury response. Using a stringent statistical assessment for differentially expressed genes (DEGs, false discovery rate FDR<0.05), we identified 282 transcripts modulated by injury in control wildtype mice injected with AAV2-*hSyn1*-Cre. Among these, 117, or 41.5%, reached this same strict threshold for differential expression in a comparison between PERK cKO retinae after injury wildtype retinae after injury (**Table S1**), with this number increased to 157, or 55.7%, using a moderately relaxed threshold of $p<0.01$ and FDR<0.2 (**Figure 2A**). All but three of these change in the opposite direction of their modulation by injury, suggesting a central role for the ISR in mediating these injury responses. Among the 154 transcripts regulated by injury in a PERK-dependent manner, 56 (36.4%) are also suppressed by ATF4 knockout, with a particularly pronounced contribution among those transcripts that are upregulated after injury (37 out of 73, or 50.7%), including seven of the nine transcripts that display CHOP-dependence at a threshold of $p<0.01$ and FDR<0.2 (**Figure 2A**). Notably, among ATF4-regulated transcripts, 86.2% also exhibit PERK-dependence at this threshold, consistent with ATF4 activation after optic nerve crush being mediated predominantly by PERK and not subject to compensation by other eIF2α kinases (Larhammar et al., 2017). This analysis, though limited by its arbitrary thresholds for defining factor-dependence, implies an essential role of the PERK-activated ISR in the transcriptional injury response, with CHOP serving as a relatively minor contributor within a program primarily mediated by ATF4.

To evaluate these relationships in a threshold-independent manner, we performed linear regression of the 282 injury-regulated genes. We first compared the impact of PERK cKO on the regulation of these transcripts by injury with that of ATF4 cKO. This analysis reveals a strong correlation (R=0.87) that, along with a best-fit slope of 0.75, suggests that the role of ATF4 in mediating the effects of PERK is more comprehensive than suggested by threshold-dependent analyses alone (**Figure 2B**). A similar assessment uncovers a milder (R=0.59), but still highly significant, correlation between PERK-dependent and CHOP-dependent injury-responsive transcripts (**Figure 2C**). However, the shallow slope of 0.23 for the best-fit line reveals that, though CHOP influences similar genes as PERK, it does so relatively mildly. Consistent with these findings, we observe a significant correlation between ATF4-dependent and CHOP-dependent transcripts, again with a shallow slope that indicates a more potent influence of ATF4 knockout (**Figure 2D**). These results imply that CHOP serves as a potentiator of the ISR after optic nerve crush rather than a primary mediator. Together, these findings are consistent with ATF4 exerting the dominant role in the transcriptional response and promotion of RGC apoptosis.

PERK signaling regulates canonical ATF4 and c-Jun transcriptional programs

To explore the transcriptional programs downstream of PERK, we next applied the Upstream Regulator tool of Ingenuity Pathway Analysis (IPA), which includes determination of potential transcription factors likely to be mediators of the observed patterns of transcriptional changes and known target genes derived from extensive curation of the literature. Consistent with previous studies (Syc-Mazurek et al., 2022; Yasuda et al., 2016), we find that ATF4, along with c-Jun, emerges among the top five candidates for a positive transcriptional regulator ($p<10^{-13}$ and Activation Z-score>2.5), based on the upregulation of many genes previously demonstrated to be direct targets of ATF4, including *Atf3*, *Mthfd2, Stc2,* and *Phgdh* (Ben-Sahra et al., 2016; Han et al., 2013; Pan et al., 2007; Zhao et al., 2016) (**Figure 3A**). IPA also suggested PGC1α (gene name: *Ppargc1a*), which can be negatively regulated by ATF4 activation (Montori-Grau et al.,

2022; Wang et al., 2013), as the most influential negative transcriptional regulator (**Table S2**). CHOP (gene name: *Ddit3*) was implicated among a cluster of dozens of less influential positive regulators ($p<10^{-5}$ and Activation Z-score>1.25) (**Figure 3A**; **Table S2**). Comparisons between wildtype and PERK (*Eif2ak3*) cKO retinae 3 days after injury suggest that disruption of PERK abrogates ATF4 activation most strongly, with c-Jun and PGC1α also affected (**Figure 3B; Table S3**). This analysis suggests the activation of a canonical PERK/ATF4-mediated transcriptional response (**Figure 3C**) after RGC axon injury and raised the unexpected possibility that PERK signaling might also influence c-Jun-regulated target genes.

To further investigate a potential interaction between c-Jun- and PERK-regulated transcripts, we leveraged RNA-seq datasets from a separate, similarly designed, study that included mice lacking c-Jun in the majority of neural retina and CHOP-null mice (Syc-Mazurek et al., 2022). First, we evaluated the expression profiles of the wildtype injury conditions between these independent studies, finding an exceptional correlation (R=0.95, Slope = 1.07) among 282 injury-regulated genes (**Figure 3D**). That robust relationship between the control conditions provided a basis for further comparisons. We therefore proceeded with a cross-study analysis comparing the impact of PERK cKO with that of c-Jun cKO. That analysis revealed a significant correlation (R=0.49; Slope = 0.44) among c-Jun- and PERK-modulated transcripts (**Figure 3E**). Nevertheless, some injury-modulated transcripts are regulated exclusively by c-Jun (*e.g.*, *Sox11* and *Arid5a*) or PERK (*e.g.*, *Chac1* and *Phgdh*). Together, these findings suggest that, despite a lack of influence of c-Jun knockout on PERK (*Eif2ak3*), ATF4 (*Atf4*), or CHOP (*Ddit3*) transcripts and vice versa, these parallel pathways participate in substantially overlapping transcriptional programs.

We next evaluated the similarity between germline and neuronal knockout of CHOP (*Ddit3*) between these two studies. Though each uncovered only a small number of CHOP-dependent, injury-responsive transcripts, those few exhibit considerable overlap. Just four transcripts passed a stringent test for CHOP-dependence in retinae of CHOP/*Ddit3*$^{-/-}$ mice

(Syc-Mazurek et al., 2022), three of which – *Stbd1*, *Gm13889*, and *Avil* (also known as Doc6 for "dependent on CHOP-6") – have been demonstrated to be upregulated neuron-autonomously by injury within RGCs by scRNA-seq (Tran et al., 2019). Using similar stringency (FDR<0.05), these three were among only five genes that we independently detected as injury-upregulated in a neuronally CHOP-dependent manner using CHOP cKO mice (**Figure 3F**). Additional injury-induced transcripts suppressed by greater than 50% in both CHOP cKO and CHOP KO (though without surpassing the FDR<0.05 threshold) include *Fibin* (p<0.0005 in both studies) and *Cdsn* (p<0.001 in both studies), genes for which ChIP-seq has previously identified CHOP binding near their transcriptional start sites under stress conditions (Han et al. 2013). These results show that, despite differences in neuroprotection between CHOP-null mice (Hu et al., 2012; Syc-Mazurek et al., 2017b) and neuronal targeting of CHOP in cKO retinae, their transcriptional consequences within the retina closely resemble one another.

Together, these expression profiles suggest that the PERK-mediated ISR is an integral contributor to the retinal transcriptional response after optic nerve injury, acting primarily through canonical ATF4 targets and interacting with c-Jun-mediated transcriptional programs.

RGC-autonomous ATF4- and CHOP-dependent transcriptional changes are prominently represented by whole retina transcriptomics

Our targeted expression of Cre recombinase in cKO mice argues for a central role for the neuronal ISR in the response to optic axon injury, with whole retina transcriptomics likely reporting both these neuron-autonomous effects and secondary consequences to other retinal cells. To determine the extent to which ISR-dependent transcription uncovered by retinal RNA-seq represents RGC-autonomous expression changes, we next leveraged an independent single-cell RNA-seq (scRNA-seq) data set that details the injury-induced expression changes within subtypes of RGCs at 2 and 4 days after optic nerve crush (Tran et al., 2019).

We began by assessing the whole retina expression of transcripts that have been demonstrated to be differentially expressed by RGCs at 2 or 4 days after optic nerve crush (pseudo-bulk scRNA-seq |Diff>0.3| and FDR<10^{-20}). Of 615 such transcripts, 597 are represented in wildtype whole retina 3 days after injury. We find that 290 of these transcripts exhibit differential expression ($|\log_2 FC|>0.25$) in retina, with all but three modulated by injury in the same direction as reported by scRNA-seq (**Figure 4A**). Moreover, the majority of the 282 injury-responsive transcripts we have identified in whole retina exhibit concordance with changes previously found by scRNA-seq of RGCs (**Supplemental Figure S2A-C**). Importantly, many transcripts identified as PERK-, ATF4-, and/or CHOP-dependent in this and other studies are among those that are upregulated neuron-autonomously within multiple subtypes of RGCs following optic nerve crush (**Figure 4B**). Accordingly, RNAScope confirms that the ATF4-dependent transcripts *Chac1, Ecel1*, and *Atf3* are elevated in the GCL in conjunction with downregulation of the RGC marker *Rbpms*, with these changes suppressed in ATF4 cKO retinae (**Figure 4C-D**). Furthermore, RNAScope corroborates that the *Avil* and *Ecel1* transcripts are upregulated in subsets of RGCs in an ATF4- and CHOP-dependent manner (**Figure 4D-E and Supplemental Figure S2D**). Consistent with this, the relationships we detected between PERK-dependent transcripts and ATF4- or c-Jun-dependent transcripts in whole retina are maintained when re-assessed using DEGs confirmed to be injury-regulated within RGCs by scRNA-seq (**Supplemental Figure S2E-F**). These results imply that the injury-induced ATF4 transcriptional program that we detect by whole retina transcriptomics of cKO mice primarily reflects RGC-autonomous expression changes.

This canonical ATF4 program, inclusive of the contribution of CHOP, contrasts with a report of two non-canonical, largely non-overlapping, programs controlled by these two ISR transcription factors (Tian et al., 2022). We next investigated potential sources of this discordance. The proposed parallel neurodegenerative programs were deduced in part by RNA-seq of FACS-enriched injured RGCs expressing gRNAs targeting ATF3 or *Ddit3*/CHOP. We

therefore began with an assessment of how the injury responses detected in whole retina in the current study compare with those reported for RGCs collected by FACS. Using only transcripts independently identified as RGC-autonomous expression changes by scRNA-seq (Tran et al. 2019) for this cross-study comparison, we find a highly significant correlation (R=0.77) between injury-regulated transcripts under control conditions (*i.e.,* without gene targeting) between these independent studies (**Supplemental Figure S3A**). This suggests that these distinct approaches similarly report prominent RGC-autonomous expression changes, inclusive of numerous known direct targets of ATF4, with a steep linear regression (slope = 2.0) that is consistent with greater sensitivity for these changes by enrichment for RGCs by FACS. Despite that similarity, linear regression reveals little correlation between the impact of cKO- and gRNA-mediated knockout on 597 RGC-autonomous, injured-regulated transcripts. We find only very weak, shallow correlation between the effects of ATF4 gRNA and *ATF4* cKO (R=0.25, slope = 0.52). cKO-sensitive signature ATF4 target genes *Chac1*, *Phgdh*, *Sesn2*, *Slc7a5,* and *Asns*, amongst others, are not among the 300 of these 598 (50.2%) transcripts reported to be significantly affected by ATF4 gRNA (**Supplemental Figure S3B**) (Crawford et al., 2015; Garaeva et al., 2016; Han et al., 2013; Liu et al., 2018; Oh-Hashi et al., 2013; Park et al., 2017). We also find no correlation between the influence of CHOP/*Ddit3* cKO and gRNA targeting CHOP, with no reported inhibition by this gRNA pool of the CHOP KO- and cKO-sensitive transcripts *Gm13889* and *Stbd1* among 333 (55.7%) significantly affected transcripts (FDR<0.05) (**Supplemental Figure S3C**)**.** Notably, the reported effects of gRNA targeting CHOP, like ATF3 gRNA, include minimal reduction of *Ddit3/*CHOP transcript but greater than 70% suppression of the pro-apoptotic and pro-regenerative *Atf3* transcript (Tian et al., 2022), an effect not observed in CHOP/*Ddit3* germline (Syc-Mazurek et al., 2022) or conditional knockout mice (present study), despite ample sensitivity for *Atf3* mRNA modulation using whole retina transcriptomics. These analyses argue that more specific and effective disruption of target genes by cKO may contribute to the striking discordance between the transcriptional programs of ATF4 and CHOP suggested by these distinct approaches.

Neuronal ATF4 knockout limits axon regeneration by PTEN-deficient RGCs

The commonalities that we uncovered between c-Jun- and PERK-regulated transcription suggested the hypothesis that, like c-Jun, PERK/ATF4 could be involved not only in promoting apoptosis but also in promoting regeneration. To investigate this possibility, we first examined the PERK- and ATF4-dependence of regeneration-associated genes (RAGs) and the injury-induced downregulation of mature and subtype-specific RGC markers, finding that many exhibit at least partial PERK- and ATF4-dependence (**Figure 5A-B**). We therefore crossed mice harboring the floxxed PTEN alleles and those harboring floxxed ATF4 alleles or floxxed PERK alleles to generate homozygous dcKO mice. Following intravitreal injection of AAV2-*hSyn1*-Cre, we performed optic nerve crush, comparing axon regeneration in these dcKO mice to that of *PTEN* cKO mice (**Figure 5C-D**). We find that neuronal PERK deficiency or ATF4 deficiency limits the efficacy of this regenerative intervention. These data support an integral contribution of the ISR to the axon regenerative program in these CNS neurons, and indicate that, as with DLK and c-Jun, ATF4 is involved in both pro-regenerative and pro-apoptotic transcriptional changes.

Discussion

Cellular stress signaling pathways typically couple the promotion of growth and repair with priming for apoptosis, a feature of stress responses that may aid in the elimination of cells that are irretrievably damaged (Hotamisligil and Davis, 2016). As prominent effectors of stress signaling, transcription factors of the bZIP family, including c-Jun and ATF3, therefore can contribute either to apoptosis or to recovery, depending on context, complicating efforts to harness transcriptional programs for axon regeneration independently of neurodegenerative programs (Jacobi et al., 2022; Kole et al., 2020; Raivich et al., 2004; Simon and Watkins, 2018; Syc-Mazurek et al., 2017b; Tian et al., 2022; Watkins et al., 2013). Multiple lines of evidence indicating that the PERK-activated ISR contributes to RGC apoptosis after optic nerve crush raised the appealing possibility that this pathway may represent a distinct branch of the injury response that might be targeted to selectively reduce neurodegeneration without suppressing repair programs (Hu et al., 2012; Larhammar et al., 2017; Tian et al., 2022; Wang et al., 2020). The cKO studies reported here, however, reveal that the PERK-activated ISR is more integral to the entire RGC injury response than previously appreciated, contributing substantially, in conjunction with c-Jun, to both apoptotic and regenerative programs. Though MAP kinase stress signaling and the ISR are known to exhibit some degree of crosstalk in other settings (Brown et al., 2016; Danzi et al., 2018; Pakos-Zebrucka et al., 2016), the exceptionally close coupling of these largely independent pathways by DLK signaling seems to be a critical feature of the response of RGCs to axon injury, with disruption of ATF4, like that of c-Jun, limiting both neurodegeneration and axon regenerative potential.

By examining in parallel the neuronal knockout of PERK and its effectors ATF4 and CHOP, along with comparisons to related studies, the current work has provided insights into the mechanisms by which the ISR influences the fates of injured RGCs. These conditional knockout mouse experiments reveal that ATF4 is the principal effector of the ISR transcriptional response, with CHOP playing a modest role within a canonical ATF4-mediated program. Though RGC

neuroprotection in germline CHOP knockout mice has long been interpreted as evidence of its central role in the neuronal ISR, our findings suggest that further investigations of CHOP may instead uncover its non-autonomous mechanisms regulating the survival of injured RGCs. The unexpectedly subtle role for neuronal CHOP aligns well with expression profiling data from CHOP-null mice (Syc-Mazurek et al., 2022) and its modest role in this study in determining RGC survival, but it appears to contrast with the more significant role for CHOP, additive with ATF4, suggested by other studies (Fang et al., 2023; Tian et al., 2022). One factor that may influence the results of CHOP cKO experiments is the ~2-fold elevated expression of a collection of eight genes (*B4galnt1*, *Slc26a10*, *Arhgef25*, *Dtx3*, *F420014N23Rik*, *Pip4k2c*, *Kif5a*, and *Dctn2*) near the *Ddit3*/CHOP locus on chromosome 10. One of those genes, *Kif5a*, is injury-responsive and alterations to its expression can influence RGC survival (Shah et al., 2022). This confound may be expected to have also been present in an independent study using the same mouse model and is therefore not likely to account for the reported differences in RGC neuroprotection (Fang et al., 2023). Though the apparent reduction of ATF3 reported for gRNA targeting *Ddit3/*CHOP, not seen in CHOP KO or cKO models, may suggest an explanation for its strikingly similar reported effects of ATF3 gRNA on the transcriptome and RGC survival, those results seem incongruent with the differential reported effects of ATF3 and CHOP gRNA on RGC axon regeneration (Jacobi et al., 2022; Tian et al., 2022). With cKO experiments revealing instead that ATF3 upregulation is dependent on ATF4 and c-Jun, it will be of interest to elucidate how much of the commonality among the transcriptional programs of these bZIP factors is attributable to interdependence of their expression and how much to their combinatorial heterodimerization. Among other non-exclusive possibilities, the commonalities between ATF4- and c-Jun-dependent transcription could reflect: (1) dependence of ATF3 elevation on c-Jun-ATF4 heterodimers; (2) dependence on ATF4 for induction of ATF3, which then heterodimerizes with c-Jun; or (3) regulation of common target genes through distinct DNA binding sites. The current study provides a framework for deciphering these networks in part by leveraging cross-study comparisons of

retina, RGC, and single-cell RNA-seq data to uncover robust RGC-autonomous expression signatures of Atf4 and other transcription factors.

Given the potential for the ISR to influence neuronal fate through multiple translational and transcriptional mechanisms, it is perhaps surprising that its primary contributions to the fates of injured RGCs are mediated by a single transcription factor, ATF4. Nevertheless, at least four lines of evidence contend that the cKO experiments reported here provide a reliable picture of its contribution. First, the extensive commonality in injury-regulated transcripts across studies, whether utilizing retinal expression data or filtering for RGC-autonomous expression changes, argues against AAV2-*hSyn1*-Cre or other technical aspects of our approach altering the injury response. Secondly, support for the modest impact of CHOP disruption on RGC injury-regulated genes is provided by the highly similar findings in the independently generated and validated CHOP-null and CHOP cKO mouse lines. Third, we find remarkable overlap between expression changes and phenotypes mediated by PERK and ATF4, which we previously demonstrated to be in the same pathway after optic nerve crush and other DLK-activating insults (Larhammar et al., 2017). Finally, the interaction between PERK/ATF4 and c-Jun-regulated transcription uncovered by our cross-study analysis predicts an impact of PERK or ATF4 knockout on RGC axon regenerative potential that is validated by dcKO with PTEN. This result is consistent with recent findings that early injury responses, including regenerative and degenerative responses that we have found in this study to be driven by PERK/ATF4, are similar in non-regenerating wildtype and regenerating PTEN-deficient RGCs (Jacobi et al, 2022). Together, these conditional knockout studies highlight the critical roles for ISR-activated transcriptional programs in determining the fates of distressed neurons and the intimate link between injury-activated neurodegenerative and axon regenerative programs.

Acknowledgements

We thank Katie Steck, Shivani Kulkarni, and Talia Sisroe for technical assistance. This work was supported by grants from Mission Connect, a project of the TIRR Foundation, NIH grants R01NS112691 and R01NS076708 to T.A.W., the Glaucoma Research Foundation, and NIH grant R00EY029360 to N.M.T. Research reported in this publication was supported by the Eunice Kennedy Shriver National Institute of Child Health & Human Development of the National Institutes of Health under Award Number P50HD103555 for use of the Neuroconnectivity Core facilities. The content is solely the responsibility of the authors and does not necessarily represent the official views of the National Institutes of Health.

Figure Legends

Figure 1. Neuronal ATF4 contributes to RGC neurodegeneration after optic nerve crush. (A) Neuronal knockout of ATF4, but not CHOP (*Ddit3*), by intravitreal AAV2-*hSyn1*-mTagBFP2-ires-Cre in conditional knockout (cKO) mice improves survival of RGCs 14 days after optic nerve crush, as assessed by immunostaining for the pan-RGC marker RBPMS. (B) Neuronal knockout of ATF4 similarly improves survival of RGCs when assessed by the robust nuclear marker of injured RGCs, phospho-c-Jun (p-c-Jun). (C-D) Comparable levels of neuroprotection are conferred by ATF4 cKO and (C) ATF4/CHOP double cKO (dcKO), or (D) *Eif2ak3* cKO, which results in deletion of the ISR-activating kinase PERK. Error bars are SEM. Statistical analysis: one-way ANOVA with Tukey's multiple comparison with a single pooled variance (*p<0.05; ***p<0.001; ****p<0.0001).

Figure 2. The PERK-activated ISR is a prominent contributor to the transcriptional response to optic nerve injury, primarily acting through ATF4. (A) Venn diagrams of 282 transcripts exhibiting significant differences by RNA-seq between uninjured retinae and 3 days after optic nerve crush (FDR<0.05). Amongst those, transcripts that exhibit differences between wildtype and cKO retinae after injury (p<0.01 and FDR<0.2) were classified as PERK-, ATF4-, or CHOP-regulated. (B-D) Linear regression analyses comparing the impact of neuronal PERK deletion (*Eif2ak3* cKO), ATF4 deletion (*Atf4* cKO), and CHOP deletion (*Ddit3* cKO) on the same 282 injury-responsive transcripts. Names of representative ATF4-dependent transcripts are burnt orange text and representative CHOP-dependent transcripts are gold text. Significant changes are indicated by colored dots (FDR<0.05).

Figure 3. PERK regulates transcriptional changes through canonical ATF4 target genes and influence on c-Jun-regulated programs. (A-B) Volcano plots of Ingenuity Pathway

Analysis (IPA) implicate ATF4 and c-Jun as potential Upstream Transcriptional Regulators of injury-induced expression changes in (A) wildtype retina, and (B) those whose activity after injury is reduced by neuronal PERK deletion. Red, orange, blue, and light blue dots indicate Z>2.5, $p<10^{-13}$; Z>1.5, $p<10^{-10}$; Z<-2.5, $p<10^{-13}$; and Z<-1.5, $p<10^{-10}$, respectively. (C) Heat map of RNA-seq data, showing known and putative ATF4 target genes after injury in wildtype or cKO retinae. (D-F) Linear regression analyses comparing current whole retina RNA-seq cKO data to published data from a similarly designed experiment (Syc-Mazurek et al, 2022). Data from that independent study is indicated on the y-axis by [&]. (D) Strong correlation among 282 injury-responsive transcripts in the respective wildtype injury conditions between these two independent studies. Names of representative ATF4-dependent transcripts are burnt orange text and representative CHOP-dependent transcripts are gold text. (E) Significant correlations between the impacts of neuronal PERK conditional knockout (this study) and deletion of c-Jun from the majority of neural retina[&] ($p<0.001$). (F) Cross-study comparison of CHOP (*Ddit3*) cKO (this study) and CHOP (*Ddit3*) KO[&] shows strong correlation between the few CHOP-dependent injury-responsive transcripts (red dots).

Figure 4. Cell-autonomous expression of ATF4- and CHOP-dependent transcripts by RGCs. (A) Volcano plot of retinal expression data three days after optic nerve crush (this study) for 597 transcripts that are significantly altered autonomously in RGCs at day 2 or day 4 after crush, as determined by scRNA-seq (Tran *et al*., 2019). 287 of these transcripts are detected at FDR<0.05 (red=upregulated, or blue=downregulated) or $|\log_2 FC|>0.25$ (light red=upregulated, or light blue=downregulated) in whole retina. Only three transcripts (yellow dots) were significantly regulated in whole retina in the discordant direction from scRNA-seq findings. (H) scRNA-seq data set (Tran *et al*., 2019) reveals RGC-autonomous activation of canonical ISR transcripts. Dot plot at 2 and 4 days after injury, showing both pan-RGC and type-specific upregulation of transcripts demonstrated by whole retina RNA-seq to be ATF4- and/or CHOP-dependent. Some

transcripts exhibiting low, non-uniform, injury induction in RGCs – *Avil*, *Gm29374*, *Cdsn*, and *Fibin* – were amongst those that appear to exhibit potential CHOP-dependence but failed to reach threshold for inclusion in either retinal injury-dependence, CHOP-dependence, or scRNA-seq pseudo-bulk analyses. (C-E) Fluorescent *in situ* hybridization (RNAScope) of ATF4- and CHOP-dependent transcripts. (C) Box-and-whisker plots of whole retina transcriptomics for selected ATF4- and CHOP-dependent transcripts and the RGC marker gene *Rbpms* that were probed by RNAScope of fresh-frozen retinal cyrosections. (D-E) Multiplex RNAScope across wildtype (WT) uninjured ("uninj") and 3 days post-crush ("3d") for three genotypes (WT, ATF4 cKO, and CHOP cKO) demonstrating prominent expression by *Rbpms*+ RGCs of injury-induced transcripts that are reduced by knockout of ATF4 (*Atf3*, *Chac1*) or by knockout of either ATF4 or CHOP (*Ecel1*, *Avil*), concordant with RNA-seq findings. Nuclei are labeled with DAPI.

Figure 5. PERK-ATF4 contributes to RGC axon regenerative potential after optic nerve crush. (A-B) Heat maps of select injury-responsive transcripts revealed by retinal RNA-seq three days after optic nerve crush in wildtype and cKO mice, focusing on (A) genes implicated in axon regeneration, and (B) the maintenance of mature and subtype-specific RGC phenotypes. (C-D) Double conditional knockout (dcKO) of neuronal PERK (*Eif2ak3*; n=4) or ATF4 (*Atf4*; n=7) reduces regeneration enabled compared to conditional knockout (cKO) of the tumor suppressor PTEN alone (n=8). Error bars are SEM. Statistical analysis: two-way ANOVA with Sidak's multiple comparisons test (**p<0.01).

Supplementary Figure Legends

Figure S1. Intravitreal AAV2-*hSyn1*-Cre results in recombination of floxxed alleles in the inner retina. (A) Whole-mount retina of *Ai14* LSL.tdTomato Cre reporter mice immunostained for two markers of RGCs (TuJ1, Brn3a). (B) Cryosections of AAV2-*hSyn1*-Cre-injuected *Ai14* retinas

reveal recombination in cells of the ganglion cell layer (GCL) and inner nuclear layer (INL). (C-D) Multiplex RNAScope of fresh-frozen retinal cryosections confirms injury-induced upregulation of *Atf4* and *Ddit3*/CHOP mRNA in the *Rbpms*$^{+}$ RGCs of the GCL that is absent in ATF4 cKO and CHOP cKO, respectively. As predicted by whole retina RNA-seq, expression of the RGC marker *Rbpms* is reduced after injury, especially in wildtype (WT) and CHOP cKO conditions. Though reduced in CHOP cKO, as predicted by whole retina RNA-seq, injury-induced *Ecel1* aids in the identification of the GCL. Nuclei are labelled with DAPI.

Figure S2. Prominent representation in RGCs of injury-responsive transcripts detected by whole retina transcriptomics. (A-C) Scatterplots showing expression level (transcripts per cell x % expressing cells) of the 282 injury-responsive genes in 3 days post ONC bulk RNA-seq identified in this study in RGC scRNA-seq dataset from Tran et al. (2019) at 1, 2, and 4 days post crush. 271/282 injury-responsive genes were detected the scRNA-seq dataset and showed a general correspondence in trend at each time point. This was most clear at 4 days post-crush (4dpc) in which 232/271 detected genes showed a >0.5 log2 fold change difference from control in the same direction as this study. Genes exhibiting >1 log2 change are labeled. This demonstrates that our expression differences from bulk-RNA seq identify RGC-specific expression changes and agree with previous pseudo-bulk analysis of RGC scRNA-seq data from similar time points. (D) Multiplex fluorescent *in situ* hybridization (RNAScope) of fresh-frozen retinal cryosections confirms that whole retina transcriptomics can even report RGC-autonomous expression of transcripts like *Avil*, which exhibits substantial injury-induced upregulation in only a subset of *Rbpms*+ RGCs in an ATF4- and CHOP-dependent manner. As predicted by whole retina RNA-seq, expression of the RGC marker *Rbpms* is reduced after injury, especially in wildtype (WT) and CHOP cKO conditions. (E-F) Similar correlations and slopes upon re-analysis of linear regression between (E) PERK- and ATF4-dependent transcripts and (F) PERK- and c-Jun-dependent transcripts using 287 genes detected as injury-responsive by both whole retina

RNA-seq (|log2FC>0.25|) and RGC scRNA-seq (Tran et al., 2019) suggests that these relationships are driven primarily by RGC-autonomous expression changes.

Figure S3. Strong concordance between this and an independent study regarding the RGC-autonomous upregulation of numerous known ATF4 target genes following optic nerve crush, but minimal concordance regarding ATF4- and CHOP-dependence. (A) Strong linear regression correlation among 597 injury-induced RGC-autonomous expression changes (as determined by scRNA-seq, Tran et al., 2019) that are detected in both whole retina (this study) and FACS-enriched RGCs (FDR<0.1, Tian et al., 2022) in control (no gene targeting) conditions. This suggests that both RNA-seq approaches readily detect RGC-autonomous changes in known ATF4 target genes (burnt orange text) and putative CHOP target genes (gold text), with greater sensitivity afforded by enriching for RGCs demonstrated by Slope>1. (B-C) Linear regression comparing the impacts of targeting (B) *Atf4* or (C) *Ddit3*/CHOP by cKO or gRNA on 597 transcripts that are significantly altered in RGCs at day 2 or day 4 after crush, as determined by scRNA-seq (Tran et al., 2019). X-axis data is from the current study (whole retina cKO), and Y-axis data is from Tian et al., 2022 (FACS-sorted RGCs expressing gRNAs), as reflected in that manuscript's Corrections (Tian et al., 2024, 2023) and corresponding updates to GEO:GSE184547 and GEO:GSE190667[#]. gRNAs significantly modulate transcripts unaffected by cKO (green dots), but do not significantly impact the expression of many transcripts impacted by cKO (blue dots).

Materials and methods

Animals

All animals used were in C57BL6/J background strain. Animal care and experimental procedures were approved by the institutional animal care and use committee (IACUC) at Baylor College of Medicine, according to NIH Guidelines.

Animal resource table

Mouse strain	Source
Atf4 cKO (*Atf4*$^{fl/fl}$) RRID:IMSR_JAX:033380	Christopher Adams, University of Iowa (Ebert et al., 2012); also available Jackson Laboratories (Strain #:033380; MGI:5550363)
Chop cKO (*Ddit3*$^{fl/fl}$) RRID:IMSR_JAX:030816	Jackson Laboratories (Strain #:030816; MGI:5781019)
Perk cKO (*Eif2ak3*$^{fl/fl}$) RRID:IMSR_JAX:023066	Jackson Laboratories (Strain #:023066; MGI:5502572)
Pten cKO (*Pten*$^{fl/fl}$) RRID:IMSR_JAX:006440	Jackson Laboratories (Strain #:006440; MGI:2156086)
Ai14 Rosa26-LSL-tdtomato RRID:IMSR_JAX:007914	Jackson Laboratories (Strain # 007914; MGI:3809524)

Antibodies resource table

Mouse strain	Source	Dilution
anti-phosphorylated-c-Jun RRID:AB_2129575	Cell Signaling Technologies #3270	1:800
anti-RBPMS	PhosphoSolutions #1832-RBPMS	1:250

RRID:AB_2492226		
anti-Tuj1 RRID:AB_10063408	Biolegend #801202	1:1250
anti-NeuN RRID:AB_2651140	Cell Signaling Technologies #24307	1:800
Alexa Fluor 647 Anti-BRN3A [EPR23257-285] RRID:AB_2916038	abcam #ab300744	1:100
Goat anti-rabbit Alexa 568	Abcam #175696	1:1000
Goat anti-guinea pig Alexa 647	Invitrogen #A21450	1:1000
Goat anti-guinea pig Alexa 488	Invitrogen #11073	1:1000

Adeno-associated virus (AAV)

Adeno-associated viral vectors containing human synapsin-1 (*hSyn1*) promoter driving expression of mTagBFP2-IRES-Cre or mTagBFP2-IRES-NLS-smGFPmyc(dark) were packaged into AAV2 capsids at the Optogenetics and Viral Vector Core at Duncan Neurological Research Institute, Houston, Texas, USA.

Intravitreal injections

Animals were anesthetized with isoflurane. Artificial tears ointment (Covetrus #11695-6832-1) was applied on the eyes. In case of bilateral injections, non-injected eye received artificial tears. The eyes were sterilized and prepared by 3 repeated applications of 5% ophthalmic betadine (Henry Schein #6900250), followed by Opti-clear ophthalmic eye wash (Akorn #NDC 17478-620-04) and wiped dry. Topical anesthetic 0.5% proparacaine HCl ophthalmic solution (Henry Schein #1365345) was applied. A 5-µl Hamilton syringe loaded with a custom 33-gauge needle (Hamilton

#7803-5) was used to puncture the eyeball and relieve some of the intraocular pressure. The Hamilton needle was inserted back into the same puncture site and 2 µl of AAV in titers ranging from 10^{12} -10^{13} vg/ml was delivered per eye.

Intra-orbital optic nerve crush (ONC)

Animals were dosed with 1mg/kg buprenorphine sustained release formulation 1 hour prior to surgery. At the time of surgery, they were anesthetized with isoflurane. Artificial tears ointment (Covetrus #11695-6832-1) was applied on the non-surgical eye. The surgical eye was sterilized and prepared by 3 repeated applications of 5% ophthalmic betadine (Henry Schein #6900250), followed by Opti-clear ophthalmic eye wash and wiped dry. Topical anesthetic 0.5% proparacaine HCl ophthalmic solution (Henry Schein #1365345) was applied on the surgical eye (left). Incisions were made in both the conjunctival layers using a pair of Vannas scissors (World precision instruments #501777). Two pairs of suture-tying forceps (Fine science tools #1106307) were used to gently clear the soft tissue in the intra-orbital space behind the eye until the optic nerve was visible. A pair of Dumont forceps (Fine science tools #1125325) were used to manually crush the optic nerve for 5s. The eyeball was gently pushed back into the orbit. Animals were then returned to their home cages and monitored until sternal recumbency was observed.

Immunolabeling of retinae

Animals were euthanized by anesthesia overdose, followed by decapitation. The eyes were harvested and fixed in 4% paraformaldehyde for 1 hour. The retinae were dissected out in 1X phosphate-buffered saline (PBS) and then blocked for 30min in 5% goat serum, 0.5% Triton X-100 and 0.025% sodium azide in 1X PBS. The retinae were then incubated for 5 days in primary antibody diluted in blocking buffer solution in 4°C. They were then washed three times in 1X PBS with 0.5% TritonX-100 for 30 min each, and then moved to appropriate secondary antibody

solution prepared in blocking buffer and incubated overnight. This was then followed by three washes again with 1X PBS with 0.5% TritonX-100 for 30 min each. Retinae were then mounted in Drop-n-Stain EverBrite™ Mounting Medium (Biotium #23008) onto slides and imaged using Zeiss Axio Imager Z1 fluorescence microscope.

Fluorescent *in situ* hybridization

Cryosections (12 μm) of fresh-frozen control retinae and retinae 3 days after optic nerve crush were subjected to RNAScope fluorescent in situ hybridization using the RNAScope Multiplex Fluorescent Reagent Kit V2 (Advanced Cell Diagnostics, Hayward, CA, USA) according to the manufacturer's protocols. The following probes were purchased from Advanced Cell Diagnostics: Mm-Rbpms-C3 (Cat No. 527231-C3), Mm-Ecel1-C2 (Cat No. 475331-C2), Mm-Ecel1-C3 (Cat No. 475331-C3), Mm-Atf4 (Cat No. 405101), Mm-Chac1 (Cat No. 514501), Mm-Avil-C2 (Cat No. 498531-C2), Mm-Atf3 (Cat No. 426891), and Mm-Ddit3 (Cat No. 317661).

RGC survival assessment

Animals that underwent optic nerve crush surgeries were euthanized two weeks post crush by anesthesia overdose, followed by decapitation. Retinae were dissected out, fixed and immunolabeled as described above. Whole mounted retinae were imaged uniformly from the periphery to the center, with 3-4 images captured at 10x per leaflet of the flat mounted retina (7-11 images per retina) in all fluorescently labeled channels. Images were blind coded and quantified for surviving RBPMS positive and/or p-c-Jun positive cells through a combination of hand counting and RGC counter tool of the Simple RGC plug-in in ImageJ FIJI. The average count of all images per retina was calculated to obtain mean cell count per image and plotted to show RGC survival. For the plot showing percentage survival of RGCs, the counts were normalized to mean count of uninjured retinae for each experimental group. Plots and statistical analyses were generated using GraphPad Prism.

Axon regeneration assessment

Animals that underwent optic nerve crush surgeries were intravitreally injected on the surgical eye with 2 µl of Alexa 594-conjugated-cholera toxin β (Life technologies #C22842) at day 14. Animals were euthanized on day 15 by anesthesia overdose followed by decapitation. Surgical eye and optic nerve were dissected out together by first cutting the optic nerves at the chiasm through intracranial dissection and making a single cut along the length of the control uninjured optic nerve. Incisions were then made in the orbital bones to remove the ceiling of the orbital cavity and gently release the surgical eye and optic nerve out together. The retinae and optic nerves were then drop fixed together in 4% PFA. The connective tissue around the optic nerves were dissected out. The optic nerves were then processed for tissue clearing by incubating in 100% methanol for 4min and then moved to Visikol-1 overnight on a shaker at 4°C. They were then moved to Visikol-2 for 2 hours with shaking at room temperature and then mounted in Visikol-2 onto slides. The whole mounted and cleared optic nerves were imaged using Zeiss Imager Z2 fluorescence microscope and Apotome 2.0. The nerves were imaged by capturing 3-5 sequential Z-stacks at 10x magnification along the length of nerve with a range of 200um and Z-stacks of 100 images each. The Z-stacks were stitched together using FIJI stitching algorithm and max intensity projections were created in FIJI. The optic nerve crush site was identified by the point where the brightest CTB labeling ends. The line tool in FIJI was used to mark regions 0.75mm and 1.5mm from the crush site. A vertical line was drawn across the optic nerve at these respective distances and the number of axons that course through the drawn line at each distance was manually counted. In regions where there were too many axons that could be accurately counted, the Z-stacks were used for quantification. Every 10th image in the z-stack was counted for number of axons coursing through the drawn lines at 0.75mm and 1.5mm from the crush site and the total

number from each Z-stack calculated to provide an estimated number of axons. Plots and statistical analyses were generated using GraphPad Prism.

RNA preparation and Next-Generation Sequencing

Animals that underwent optic nerve crush surgeries were euthanized 3 days post crush by anesthesia overdose and decapitation. The retinae were quickly dissected out in 1X PBS and snap frozen in dry ice-ethanol bath and stored in -80°C until ready to be processed for RNA extraction. RNA was extracted using the Qiagen RNeasy micro kit (#74004). Extracted RNA was sent to Novogene Co. Ltd (Beijing, China) for Next Generation Sequencing using their Illumina NovaSeq platform for mouse mRNA sequencing. RNA libraries were prepared according to Novogene procedures by polyA capture (or rRNA removal) and reverse transcription of cDNA. Illumina PE150 technology was employed to sequence the samples. Sample reads were aligned to mouse reference genome using HISAT2 algorithm. Gene expression analysis was performed using Novogene pipeline. Venn diagrams were generated using DeepVenn (Hulsen, 2022), heatmaps were generated using Morpheus (https://software.broadinstitute.org/morpheus), pathway analyses were performed using Ingenuity pathway analysis (Qiagen) and single cell mouse retinal ganglion cell atlas was obtained from Broad Single Cell Portal (Tarhan et al., 2023). Cross-study analyses of RNA-seq findings were performed using logFC and FDR values reported for c-Jun cKO and CHOP KO mice (Syc-Mazurek et al., 2022) and after performing an independent DESeq2 analysis of GSE190667 and GSE184547 FASTQ (Tian et al., 2024, 2023, 2022) uploading directly from GEO to the OneStopRNAseq resource (Li et al., 2020).

Data availability

RNA-sequencing data is available from the Gene Expression Omnibus through series accession number GEO: GSE223321.

References

Asghari Adib E, Smithson LJ, Collins CA. 2018. An axonal stress response pathway: degenerative and regenerative signaling by DLK. *Curr Opin Neurobiol* **53**:110–119. doi:10.1016/j.conb.2018.07.002

Ben-Sahra I, Hoxhaj G, Ricoult SJH, Asara JM, Manning BD. 2016. mTORC1 induces purine synthesis through control of the mitochondrial tetrahydrofolate cycle. *Science* **351**:728–733. doi:10.1126/science.aad0489

Brown M, Strudwick N, Suwara M, Sutcliffe LK, Mihai AD, Ali AA, Watson JN, Schröder M. 2016. An initial phase of JNK activation inhibits cell death early in the endoplasmic reticulum stress response. *J Cell Sci* **129**:2317–2328. doi:10.1242/jcs.179127

Crawford RR, Prescott ET, Sylvester CF, Higdon AN, Shan J, Kilberg MS, Mungrue IN. 2015. Human CHAC1 protein degrades glutathione, and mRNA induction Is regulated by the transcription factors ATF4 and ATF3 and a bipartite ATF/CRE regulatory element. *J Biol Chem* **290**:15878–15891. doi:10.1074/jbc.M114.635144

Danzi MC, Mehta ST, Dulla K, Zunino G, Cooper DJ, Bixby JL, Lemmon VP. 2018. The effect of Jun dimerization on neurite outgrowth and motif binding. *Mol Cell Neurosci* **92**:114–127. doi:10.1016/j.mcn.2018.08.001

Fang F, Liu P, Huang H, Feng X, Li L, Sun Y, Kaufman RJ, Hu Y. 2023. RGC-specific ATF4 and/or CHOP deletion rescues glaucomatous neurodegeneration and visual function. *Mol Ther Nucleic Acids* **33**:286–295. doi:10.1016/j.omtn.2023.07.015

Farley MM, Watkins TA. 2018. Intrinsic neuronal stress response pathways in injury and disease. *Annu Rev Pathol* **13**:93–116. doi:10.1146/annurev-pathol-012414-040354

Garaeva AA, Kovaleva IE, Chumakov PM, Evstafieva AG. 2016. Mitochondrial dysfunction induces SESN2 gene expression through Activating Transcription Factor 4. *Cell Cycle* **15**:64–71. doi:10.1080/15384101.2015.1120929

Han J, Back SH, Hur J, Lin Y-H, Gildersleeve R, Shan J, Yuan CL, Krokowski D, Wang S, Hatzoglou M, Kilberg MS, Sartor MA, Kaufman RJ. 2013. ER-stress-induced transcriptional regulation increases protein synthesis leading to cell death. *Nat Cell Biol* **15**:481–490. doi:10.1038/ncb2738

Hotamisligil GS, Davis RJ. 2016. Cell signaling and stress responses. *Cold Spring Harb Perspect Biol* **8**. doi:10.1101/cshperspect.a006072

Hulsen T. 2022. DeepVenn -- a web application for the creation of area-proportional Venn diagrams using the deep learning framework Tensorflow.js. *arXiv*. doi:10.48550/arxiv.2210.04597

Hu Y, Park KK, Yang L, Wei X, Yang Q, Cho K-S, Thielen P, Lee A-H, Cartoni R, Glimcher LH, Chen DF, He Z. 2012. Differential effects of unfolded protein response pathways on axon injury-induced death of retinal ganglion cells. *Neuron* **73**:445–452. doi:10.1016/j.neuron.2011.11.026

Jacobi A, Tran NM, Yan W, Benhar I, Tian F, Schaffer R, He Z, Sanes JR. 2022. Overlapping transcriptional programs promote survival and axonal regeneration of injured retinal ganglion cells. *Neuron* **110**:2625-2645.e7. doi:10.1016/j.neuron.2022.06.002

Kole C, Brommer B, Nakaya N, Sengupta M, Bonet-Ponce L, Zhao T, Wang C, Li W, He Z, Tomarev S. 2020. Activating transcription factor 3 (ATF3) protects retinal ganglion cells and promotes functional preservation after optic nerve crush. *Invest Ophthalmol Vis Sci* **61**:31. doi:10.1167/iovs.61.2.31

Larhammar M, Huntwork-Rodriguez S, Jiang Z, Solanoy H, Sengupta Ghosh A, Wang B, Kaminker JS, Huang K, Eastham-Anderson J, Siu M, Modrusan Z, Farley MM, Tessier-Lavigne M, Lewcock JW, Watkins TA. 2017. Dual leucine zipper kinase-dependent PERK activation contributes to neuronal degeneration following insult. *eLife* **6**. doi:10.7554/eLife.20725

Le Pichon CE, Meilandt WJ, Dominguez S, Solanoy H, Lin H, Ngu H, Gogineni A, Sengupta Ghosh A, Jiang Z, Lee S-H, Maloney J, Gandham VD, Pozniak CD, Wang B, Lee S, Siu M, Patel S, Modrusan Z, Liu X, Rudhard Y, Baca M, Gustafson A, Kaminker J, Carano RAD, Huang EJ, Foreman O, Weimer R, Scearce-Levie K, Lewcock JW. 2017. Loss of dual leucine zipper kinase signaling is protective in animal models of neurodegenerative disease. *Sci Transl Med* **9**. doi:10.1126/scitranslmed.aag0394

Lindborg JA, Tran NM, Chenette DM, DeLuca K, Foli Y, Kannan R, Sekine Y, Wang X, Wollan M, Kim I-J, Sanes JR, Strittmatter SM. 2021. Optic nerve regeneration screen identifies multiple genes restricting adult neural repair. *Cell Rep* **34**:108777. doi:10.1016/j.celrep.2021.108777

Liu J, Amar F, Corona C, So RWL, Andrews SJ, Nagy PL, Shelanski ML, Greene LA. 2018. Brain-Derived Neurotrophic Factor Elevates Activating Transcription Factor 4 (ATF4) in Neurons and Promotes ATF4-Dependent Induction of Sesn2. *Front Mol Neurosci* **11**:62. doi:10.3389/fnmol.2018.00062

Li R, Hu K, Liu H, Green MR, Zhu LJ. 2020. OneStopRNAseq: A Web Application for Comprehensive and Efficient Analyses of RNA-Seq Data. *Genes* **11**. doi:10.3390/genes11101165

Montori-Grau M, Aguilar-Recarte D, Zarei M, Pizarro-Delgado J, Palomer X, Vázquez-Carrera M. 2022. Endoplasmic reticulum stress downregulates PGC-1α in skeletal muscle through ATF4 and an mTOR-mediated reduction of CRTC2. *Cell Commun Signal* **20**:53. doi:10.1186/s12964-022-00865-9

Oh-Hashi K, Nomura Y, Shimada K, Koga H, Hirata Y, Kiuchi K. 2013. Transcriptional and post-translational regulation of mouse cation transport regulator homolog 1. *Mol Cell Biochem* **380**:97–106. doi:10.1007/s11010-013-1663-1

Pakos-Zebrucka K, Koryga I, Mnich K, Ljujic M, Samali A, Gorman AM. 2016. The integrated stress response. *EMBO Rep* **17**:1374–1395. doi:10.15252/embr.201642195

Pan Y-X, Chen H, Thiaville MM, Kilberg MS. 2007. Activation of the ATF3 gene through a co-ordinated amino acid-sensing response programme that controls transcriptional regulation of responsive genes following amino acid limitation. *Biochem J* **401**:299–307. doi:10.1042/BJ20061261

Park Y, Reyna-Neyra A, Philippe L, Thoreen CC. 2017. mTORC1 Balances Cellular Amino Acid Supply with Demand for Protein Synthesis through Post-transcriptional Control of ATF4. *Cell Rep* **19**:1083–1090. doi:10.1016/j.celrep.2017.04.042

Patel AK, Broyer RM, Lee CD, Lu T, Louie MJ, La Torre A, Al-Ali H, Vu MT, Mitchell KL, Wahlin KJ, Berlinicke CA, Jaskula-Ranga V, Hu Y, Duan X, Vilar S, Bixby JL, Weinreb RN, Lemmon VP, Zack DJ, Welsbie DS. 2020. Inhibition of GCK-IV kinases dissociates cell death and axon regeneration in CNS neurons. *Proc Natl Acad Sci USA* **117**:33597–33607. doi:10.1073/pnas.2004683117

Pitale PM, Gorbatyuk O, Gorbatyuk M. 2017. Neurodegeneration: keeping ATF4 on a tight leash. *Front Cell Neurosci* **11**:410. doi:10.3389/fncel.2017.00410

Raivich G, Bohatschek M, Da Costa C, Iwata O, Galiano M, Hristova M, Nateri AS, Makwana M, Riera-Sans L, Wolfer DP, Lipp H-P, Aguzzi A, Wagner EF, Behrens A. 2004. The AP-1 transcription factor c-Jun is required for efficient axonal regeneration. *Neuron* **43**:57–67. doi:10.1016/j.neuron.2004.06.005

Shah SH, Schiapparelli LM, Ma Y, Yokota S, Atkins M, Xia X, Cameron EG, Huang T, Saturday S, Sun CB, Knasel C, Blackshaw S, Yates JR, Cline HT, Goldberg JL. 2022. Quantitative transportomics identifies Kif5a as a major regulator of neurodegeneration. *eLife* **11**. doi:10.7554/eLife.68148

Simon DJ, Watkins TA. 2018. Therapeutic opportunities and pitfalls in the treatment of axon degeneration. *Curr Opin Neurol* **31**:693–701. doi:10.1097/WCO.0000000000000621

Syc-Mazurek SB, Fernandes KA, Libby RT. 2017a. JUN is important for ocular hypertension-induced retinal ganglion cell degeneration. *Cell Death Dis* **8**:e2945. doi:10.1038/cddis.2017.338

Syc-Mazurek SB, Fernandes KA, Wilson MP, Shrager P, Libby RT. 2017b. Together JUN and DDIT3 (CHOP) control retinal ganglion cell death after axonal injury. *Mol Neurodegener* **12**:71. doi:10.1186/s13024-017-0214-8

Syc-Mazurek SB, Yang HS, Marola OJ, Howell GR, Libby RT. 2022. Transcriptional control of retinal ganglion cell death after axonal injury. *Cell Death Dis* **13**:244. doi:10.1038/s41419-022-04666-3

Tarhan L, Bistline J, Chang J, Galloway B, Hanna E, Weitz E. 2023. Single Cell Portal: an interactive home for single-cell genomics data. *BioRxiv*. doi:10.1101/2023.07.13.548886

Tian F, Cheng Y, Zhou S, Wang Qianbin, Monavarfeshani A, Gao K, Jiang W, Kawaguchi R, Wang Qing, Tang M, Donahue R, Meng H, Zhang Y, Jacobi A, Yan W, Yin J, Cai X, Yang Z, Hegarty S, Stanicka J, Dmitriev P, Taub D, Zhu J, Woolf CJ, Sanes JR, Geschwind DH, He Z. 2024. Core transcription programs controlling injury-induced neurodegeneration of retinal ganglion cells. *Neuron* **112**:2453–2456. doi:10.1016/j.neuron.2024.06.009

Tian F, Cheng Y, Zhou S, Wang Qianbin, Monavarfeshani A, Gao K, Jiang W, Kawaguchi R, Wang Qing, Tang M, Donahue R, Meng H, Zhang Y, Jacobi A, Yan W, Yin J, Cai X, Yang Z, Hegarty S, Stanicka J, Dmitriev P, Taub D, Zhu J, Woolf CJ, Sanes JR, Geschwind DH, He Z. 2023. Core transcription programs controlling injury-induced neurodegeneration of retinal ganglion cells. *Neuron* **111**:444. doi:10.1016/j.neuron.2023.01.008

Tian F, Cheng Y, Zhou S, Wang Qianbin, Monavarfeshani A, Gao K, Jiang W, Kawaguchi R, Wang Qing, Tang M, Donahue R, Meng H, Zhang Y, Jacobi A, Yan W, Yin J, Cai X, Yang Z, Hegarty S, Stanicka J, Dmitriev P, Taub D, Zhu J, Woolf CJ, Sanes JR, Geschwind DH, He Z. 2022. Core transcription programs controlling injury-induced neurodegeneration of retinal ganglion cells. *Neuron* **110**:2607-2624.e8. doi:10.1016/j.neuron.2022.06.003

Tran NM, Shekhar K, Whitney IE, Jacobi A, Benhar I, Hong G, Yan W, Adiconis X, Arnold ME, Lee JM, Levin JZ, Lin D, Wang C, Lieber CM, Regev A, He Z, Sanes JR. 2019. Single-Cell Profiles of Retinal Ganglion Cells Differing in Resilience to Injury Reveal Neuroprotective Genes. *Neuron* **104**:1039-1055.e12. doi:10.1016/j.neuron.2019.11.006

Vidal-Sanz M, Galindo-Romero C, Valiente-Soriano FJ, Nadal-Nicolás FM, Ortin-Martinez A, Rovere G, Salinas-Navarro M, Lucas-Ruiz F, Sanchez-Migallon MC, Sobrado-Calvo P, Aviles-Trigueros M, Villegas-Pérez MP, Agudo-Barriuso M. 2017. Shared and Differential Retinal Responses against Optic Nerve Injury and Ocular Hypertension. *Front Neurosci* **11**:235. doi:10.3389/fnins.2017.00235

Wang C, Xia T, Du Y, Meng Q, Li H, Liu B, Chen S, Guo F. 2013. Effects of ATF4 on PGC1α expression in brown adipose tissue and metabolic responses to cold stress. *Metab Clin Exp* **62**:282–289. doi:10.1016/j.metabol.2012.07.017

Wang Q, Zhuang P, Huang H, Li L, Liu L, Webber HC, Dalal R, Siew L, Fligor CM, Chang K-C, Nahmou M, Kreymerman A, Sun Y, Meyer JS, Goldberg JL, Hu Y. 2020. Mouse γ-Synuclein Promoter-Mediated Gene Expression and Editing in Mammalian Retinal Ganglion Cells. *J Neurosci* **40**:3896–3914. doi:10.1523/JNEUROSCI.0102-20.2020

Watkins TA, Wang B, Huntwork-Rodriguez S, Yang J, Jiang Z, Eastham-Anderson J, Modrusan Z, Kaminker JS, Tessier-Lavigne M, Lewcock JW. 2013. DLK initiates a transcriptional program that couples apoptotic and regenerative responses to axonal injury. *Proc Natl Acad Sci USA* **110**:4039–4044. doi:10.1073/pnas.1211074110

Welsbie DS, Mitchell KL, Jaskula-Ranga V, Sluch VM, Yang Z, Kim J, Buehler E, Patel A, Martin SE, Zhang P-W, Ge Y, Duan Y, Fuller J, Kim B-J, Hamed E, Chamling X, Lei L, Fraser IDC, Ronai ZA, Berlinicke CA, Zack DJ. 2017. Enhanced Functional Genomic Screening Identifies Novel Mediators of Dual Leucine Zipper Kinase-Dependent Injury Signaling in Neurons. *Neuron* **94**:1142-1154.e6. doi:10.1016/j.neuron.2017.06.008

Welsbie DS, Yang Z, Ge Y, Mitchell KL, Zhou X, Martin SE, Berlinicke CA, Hackler L, Fuller J, Fu J, Cao L, Han B, Auld D, Xue T, Hirai S, Germain L, Simard-Bisson C, Blouin R, Nguyen JV, Davis CO, Enke RA, Boye SL, Merbs SL, Marsh-Armstrong N, Hauswirth WW, DiAntonio A, Nickells RW, Inglese J, Hanes J, Yau K-W, Quigley HA, Zack DJ. 2013. Functional genomic screening identifies dual leucine zipper kinase as a key mediator of retinal ganglion cell death. *Proc Natl Acad Sci USA* **110**:4045–4050. doi:10.1073/pnas.1211284110

Yang L, Li S, Miao L, Huang H, Liang F, Teng X, Xu L, Wang Q, Xiao W, Ridder WH, Ferguson TA, Chen DF, Kaufman RJ, Hu Y. 2016. Rescue of glaucomatous neurodegeneration by differentially modulating neuronal endoplasmic reticulum stress molecules. *J Neurosci* **36**:5891–5903. doi:10.1523/JNEUROSCI.3709-15.2016

Yasuda M, Tanaka Y, Omodaka K, Nishiguchi KM, Nakamura O, Tsuda S, Nakazawa T. 2016. Transcriptome profiling of the rat retina after optic nerve transection. *Sci Rep* **6**:28736. doi:10.1038/srep28736

Zhao E, Ding J, Xia Y, Liu M, Ye B, Choi J-H, Yan C, Dong Z, Huang S, Zha Y, Yang L, Cui H, Ding H-F. 2016. KDM4C and ATF4 cooperate in transcriptional control of amino acid metabolism. *Cell Rep* **14**:506–519. doi:10.1016/j.celrep.2015.12.053

Figure 1

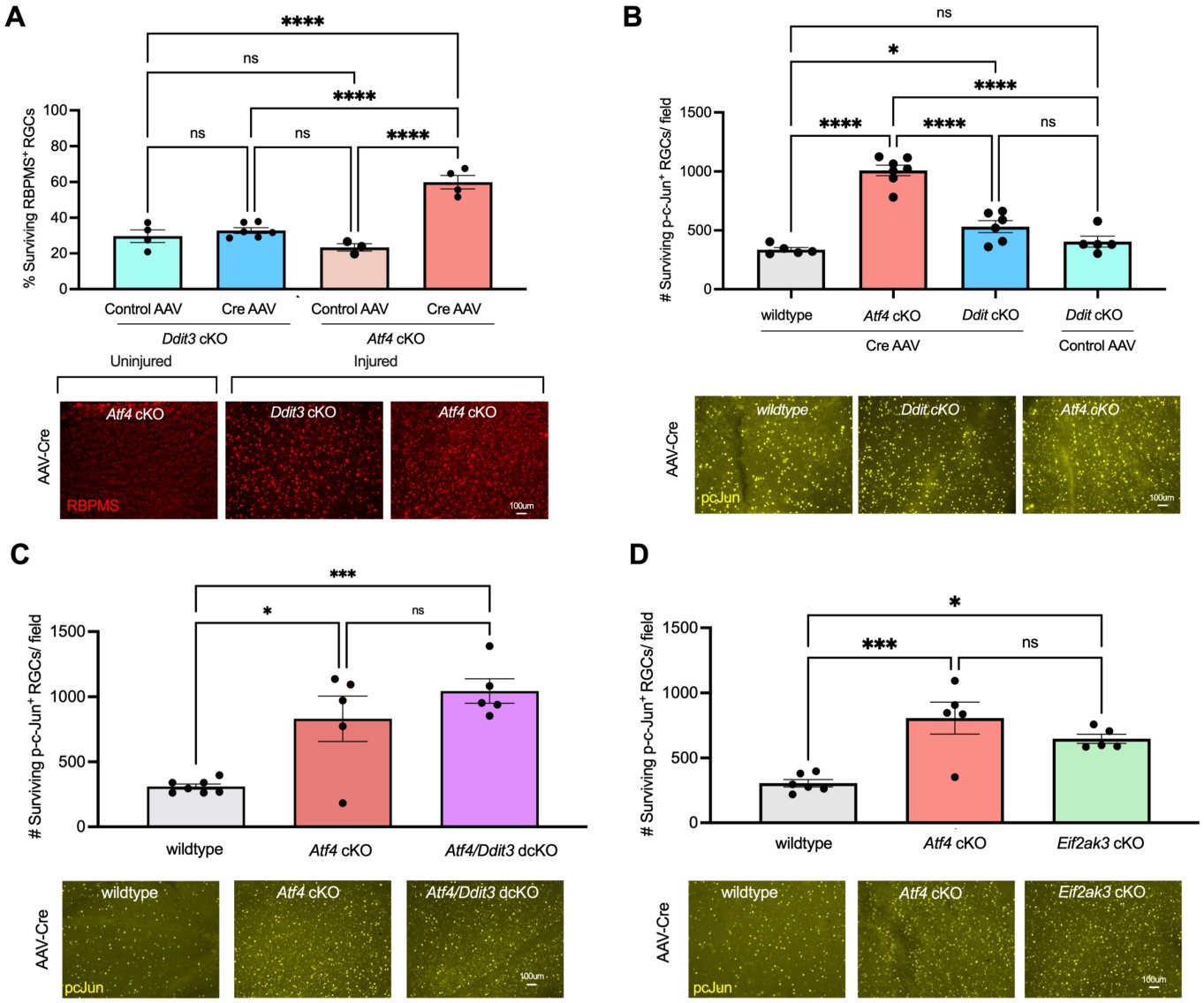
A
% Surviving RBPMS+ RGCs
100
80
60
40
20
0
****
ns
****
ns
ns
****
Control AAV
Cre AAV
Control AAV
Cre AAV
Ddit3 cKO
Atf4 cKO
Uninjured
Injured
AAV-Cre
Atf4 cKO
Ddit3 cKO
Atf4 cKO
RBPMS
100um
B
Surviving p-c-Jun+ RGCs/ field
1500
1000
500
0
ns
*
****
****
****
ns
wildtype
Atf4 cKO
Ddit cKO
Ddit cKO
Cre AAV
Control AAV
AAV-Cre
wildtype
Ddit cKO
Atf4 cKO
pcJun
100um
C
Surviving p-c-Jun+ RGCs/ field
1500
1000
500
0
***
*
ns
wildtype
Atf4 cKO
Atf4/Ddit3 dcKO
AAV-Cre
wildtype
Atf4 cKO
Atf4/Ddit3 dcKO
pcJun
100um
D
Surviving p-c-Jun+ RGCs/ field
1500
1000
500
0
*
***
ns
wildtype
Atf4 cKO
Eif2ak3 cKO
AAV-Cre
wildtype
Atf4 cKO
Eif2ak3 cKO
pcJun
100um

Figure 2

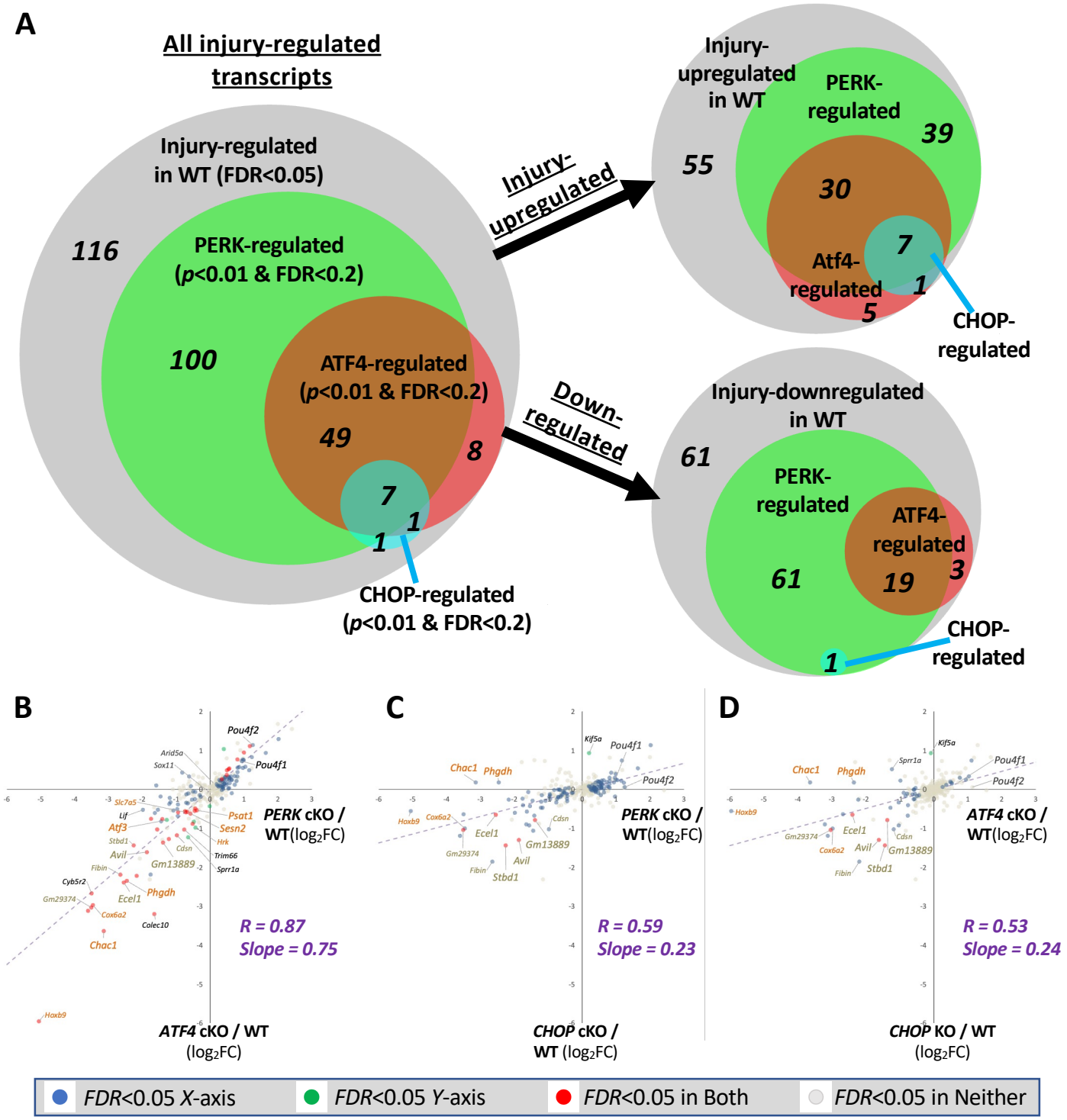
A
All injury-regulated transcripts
Injury-regulated in WT (FDR<0.05)
116
PERK-regulated (p<0.01 & FDR<0.2)
100
ATF4-regulated (p<0.01 & FDR<0.2)
49
8
7
1
1
CHOP-regulated (p<0.01 & FDR<0.2)
Injury-upregulated
Injury-upregulated in WT
55
PERK-regulated
39
30
7
Atf4-regulated
1
5
CHOP-regulated
Down-regulated
Injury-downregulated in WT
61
PERK-regulated
61
ATF4-regulated
19
3
1
CHOP-regulated
B
Pou4f2
Pou4f1
Psat1
Sesn2
Hrk
Trim66
Sprr1a
Arid5a
Sox11
Slc7a5
Lif
Atf3
Stbd1
Avil
Fibin
Cdsn
Gm13889
Cyb5r2
Gm29374
Ecel1
Phgdh
Cox6a2
Colec10
Chac1
Hoxb9
PERK cKO / WT(log2FC)
R = 0.87
Slope = 0.75
ATF4 cKO / WT (log2FC)
C
Kif5a
Pou4f1
Pou4f2
Chac1
Phgdh
Hoxb9
Cox6a2
Ecel1
Cdsn
Gm13889
Gm29374
Avil
Fibin
Stbd1
PERK cKO / WT(log2FC)
R = 0.59
Slope = 0.23
CHOP cKO / WT (log2FC)
D
Kif5a
Sprr1a
Pou4f1
Pou4f2
Chac1
Phgdh
Hoxb9
Gm29374
Ecel1
Cdsn
Cox6a2
Avil
Gm13889
Fibin
Stbd1
ATF4 cKO / WT(log2FC)
R = 0.53
Slope = 0.24
CHOP KO / WT (log2FC)
FDR<0.05 X-axis
FDR<0.05 Y-axis
FDR<0.05 in Both
FDR<0.05 in Neither

Figure 3

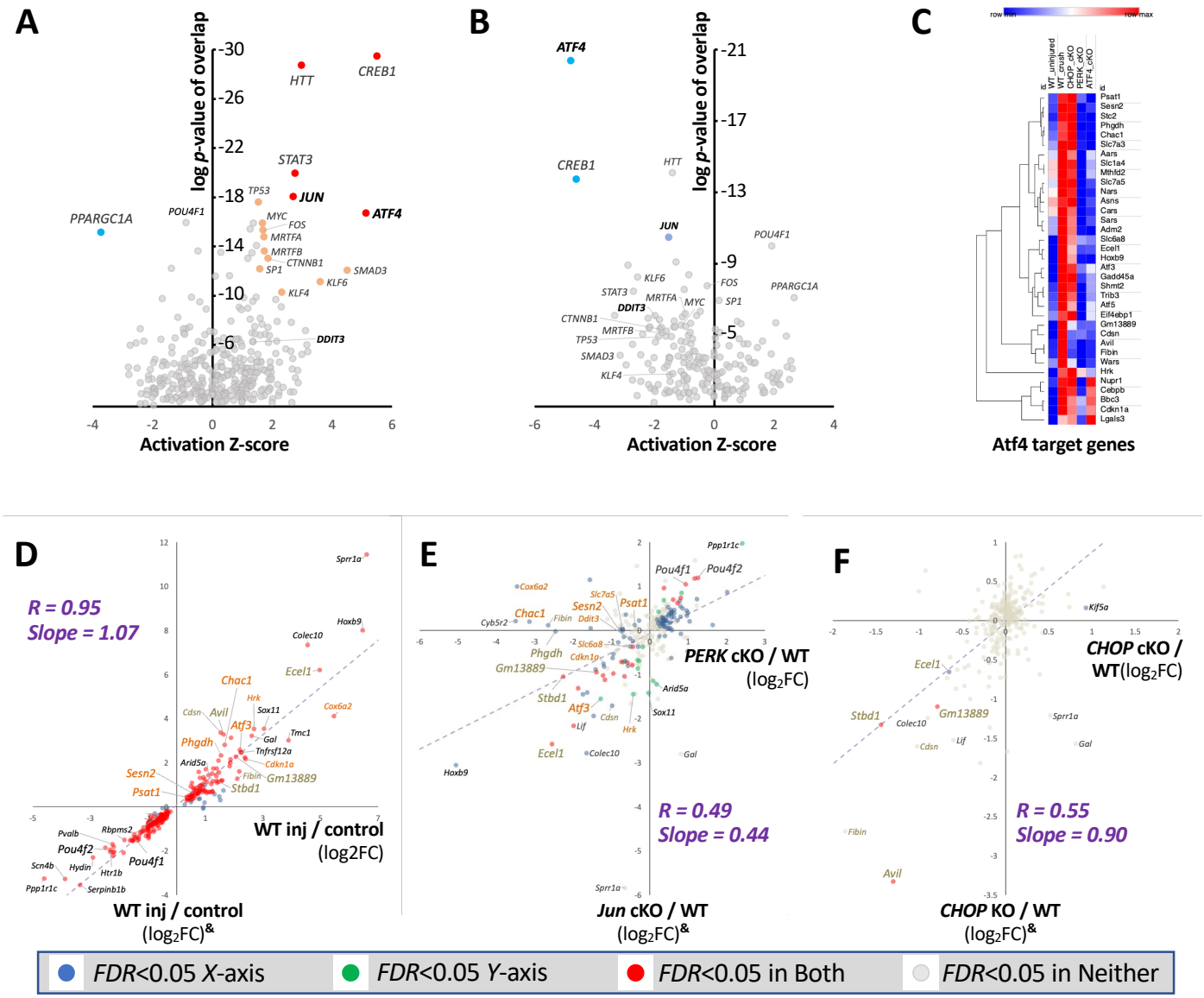
A
log p-value of overlap
Activation Z-score
HTT
CREB1
STAT3
JUN
ATF4
TP53
POU4F1
PPARGC1A
MYC
FOS
MRTFA
MRTFB
CTNNB1
SP1
SMAD3
KLF6
KLF4
DDIT3
B
ATF4
CREB1
HTT
JUN
POU4F1
KLF6
STAT3
MRTFA
MYC
DDIT3
FOS
SP1
PPARGC1A
CTNNB1
MRTFB
TP53
SMAD3
KLF4
C
Atf4 target genes
D
R = 0.95
Slope = 1.07
WT inj / control
(log2FC)
WT inj / control
(log2FC)&
E
PERK cKO / WT
(log2FC)
R = 0.49
Slope = 0.44
Jun cKO / WT
(log2FC)&
F
CHOP cKO /
WT(log2FC)
R = 0.55
Slope = 0.90
CHOP KO / WT
(log2FC)&
FDR<0.05 X-axis
FDR<0.05 Y-axis
FDR<0.05 in Both
FDR<0.05 in Neither

Figure 4

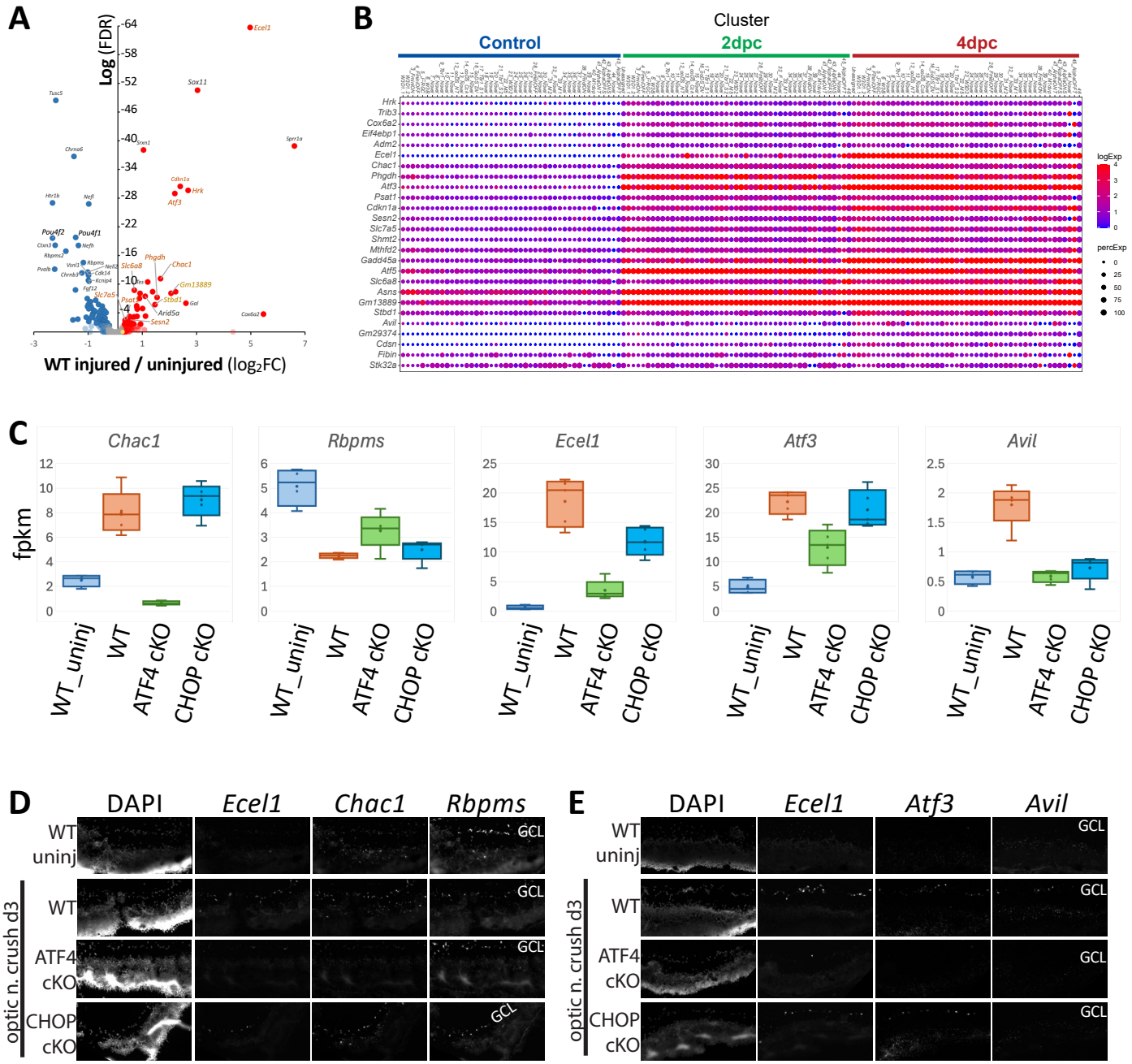
A
Log (FDR)
WT injured / uninjured (log2FC)
Ecel1
Sox11
Sprr1a
Cdkn1a
Hrk
Atf3
Phgdh
Chac1
Gm13889
Slc6a8
Psat1
Stbd1
Gal
Arid5a
Sesn2
Cox6a2
Tusc5
Chrna6
Htr1b
Nefl
Pou4f2
Pou4f1
B
Cluster
Control
2dpc
4dpc
Hrk
Trib3
Cox6a2
Eif4ebp1
Adm2
Ecel1
Chac1
Phgdh
Atf3
Psat1
Cdkn1a
Sesn2
Slc7a5
Shmt2
Mthfd2
Gadd45a
Atf5
Slc6a8
Asns
Gm13889
Stbd1
Avil
Gm29374
Cdsn
Fibin
Stk32a
logExp
percExp
C
Chac1
Rbpms
Ecel1
Atf3
Avil
fpkm
WT_uninj
WT
ATF4 cKO
CHOP cKO
D
DAPI
Ecel1
Chac1
Rbpms
WT uninj
WT
ATF4 cKO
CHOP cKO
optic n. crush d3
GCL
E
DAPI
Ecel1
Atf3
Avil
WT uninj
WT
ATF4 cKO
CHOP cKO
optic n. crush d3
GCL

Figure 5

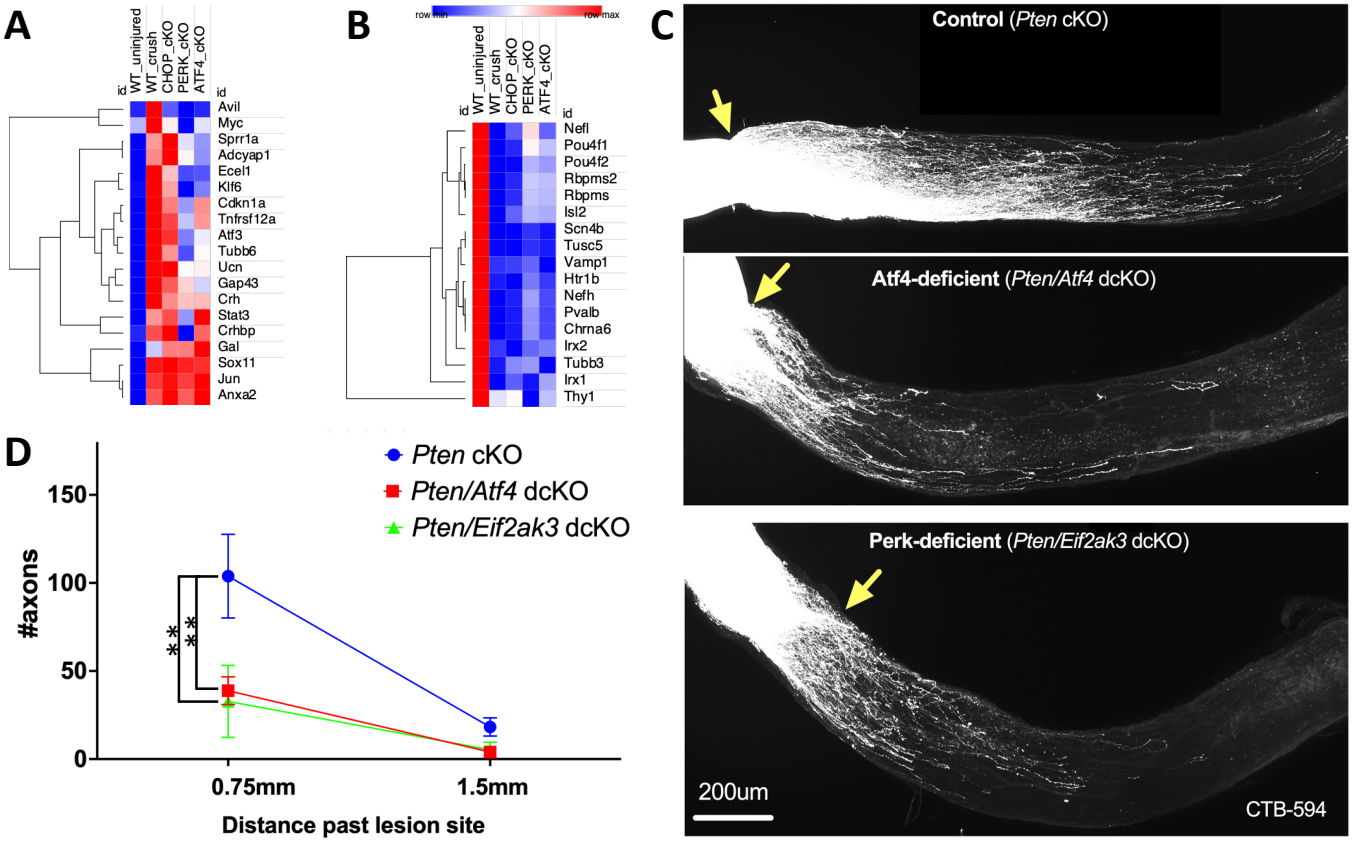
A
id
WT_uninjured
WT_crush
CHOP_cKO
PERK_cKO
ATF4_cKO
id
Avil
Myc
Sprr1a
Adcyap1
Ecel1
Klf6
Cdkn1a
Tnfrsf12a
Atf3
Tubb6
Ucn
Gap43
Crh
Stat3
Crhbp
Gal
Sox11
Jun
Anxa2
B
row min
row max
id
WT_uninjured
WT_crush
CHOP_cKO
PERK_cKO
ATF4_cKO
id
Nefl
Pou4f1
Pou4f2
Rbpms2
Rbpms
Isl2
Scn4b
Tusc5
Vamp1
Htr1b
Nefh
Pvalb
Chrna6
Irx2
Tubb3
Irx1
Thy1
C
Control (Pten cKO)
Atf4-deficient (Pten/Atf4 dcKO)
Perk-deficient (Pten/Eif2ak3 dcKO)
200um
CTB-594
D
Pten cKO
Pten/Atf4 dcKO
Pten/Eif2ak3 dcKO
#axons
150
100
50
0
***
***
0.75mm
1.5mm
Distance past lesion site

Figure S1

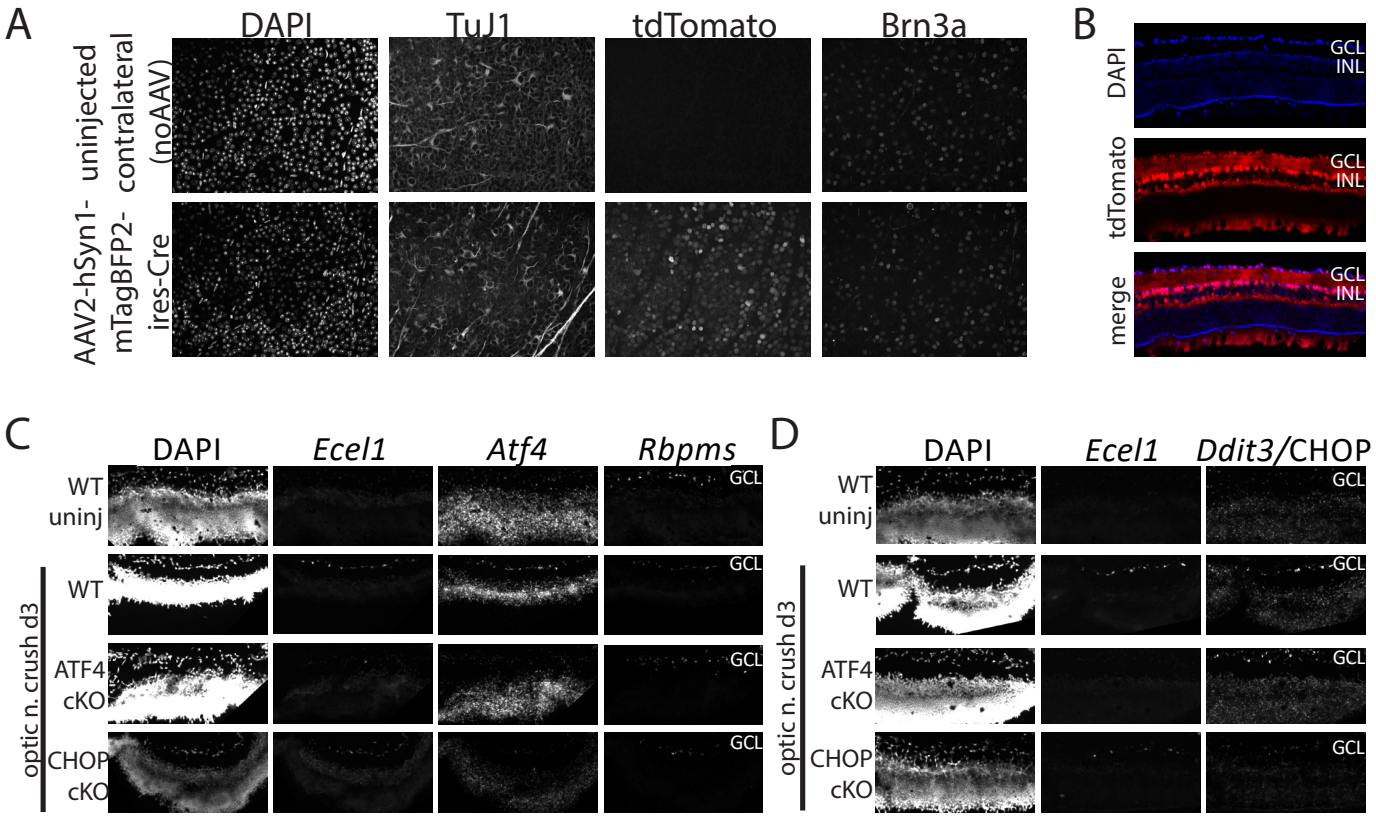
A
DAPI
TuJ1
tdTomato
Brn3a
uninjected contralateral (noAAV)
AAV2-hSyn1-mTagBFP2-ires-Cre
B
DAPI
tdTomato
merge
GCL
INL
C
DAPI
Ecel1
Atf4
Rbpms
WT uninj
optic n. crush d3
WT
ATF4 cKO
CHOP cKO
GCL
D
DAPI
Ecel1
Ddit3/CHOP
WT uninj
optic n. crush d3
WT
ATF4 cKO
CHOP cKO
GCL

Figure S2

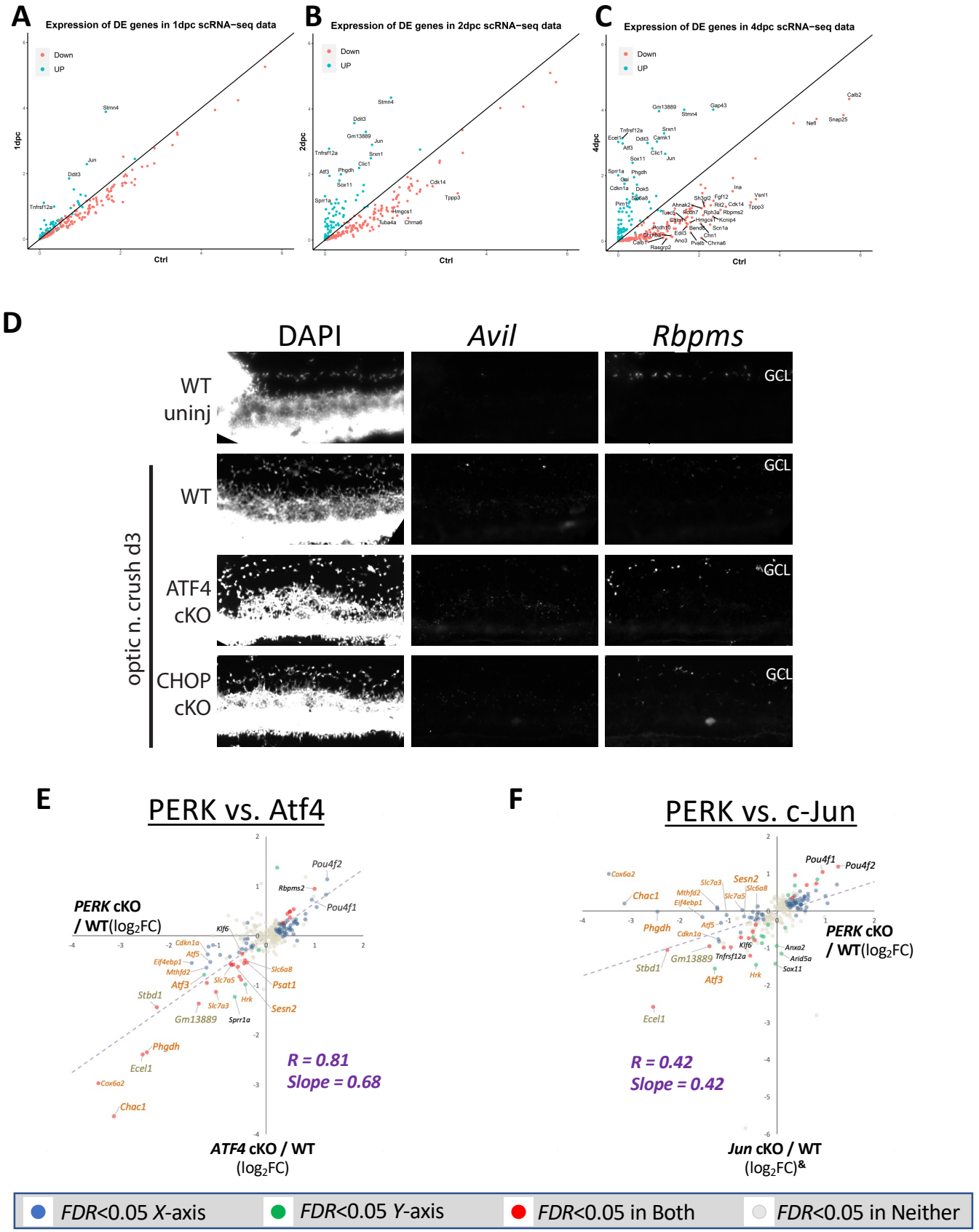
A
Expression of DE genes in 1dpc scRNA−seq data
Down
UP
1dpc
Ctrl
B
Expression of DE genes in 2dpc scRNA−seq data
2dpc
C
Expression of DE genes in 4dpc scRNA−seq data
4dpc
D
DAPI
Avil
Rbpms
WT uninj
WT
ATF4 cKO
CHOP cKO
optic n. crush d3
GCL
E
PERK vs. Atf4
PERK cKO / WT(log2FC)
ATF4 cKO / WT (log2FC)
R = 0.81
Slope = 0.68
F
PERK vs. c-Jun
PERK cKO / WT(log2FC)
Jun cKO / WT (log2FC)&
R = 0.42
Slope = 0.42
FDR<0.05 X-axis
FDR<0.05 Y-axis
FDR<0.05 in Both
FDR<0.05 in Neither

Figure S3

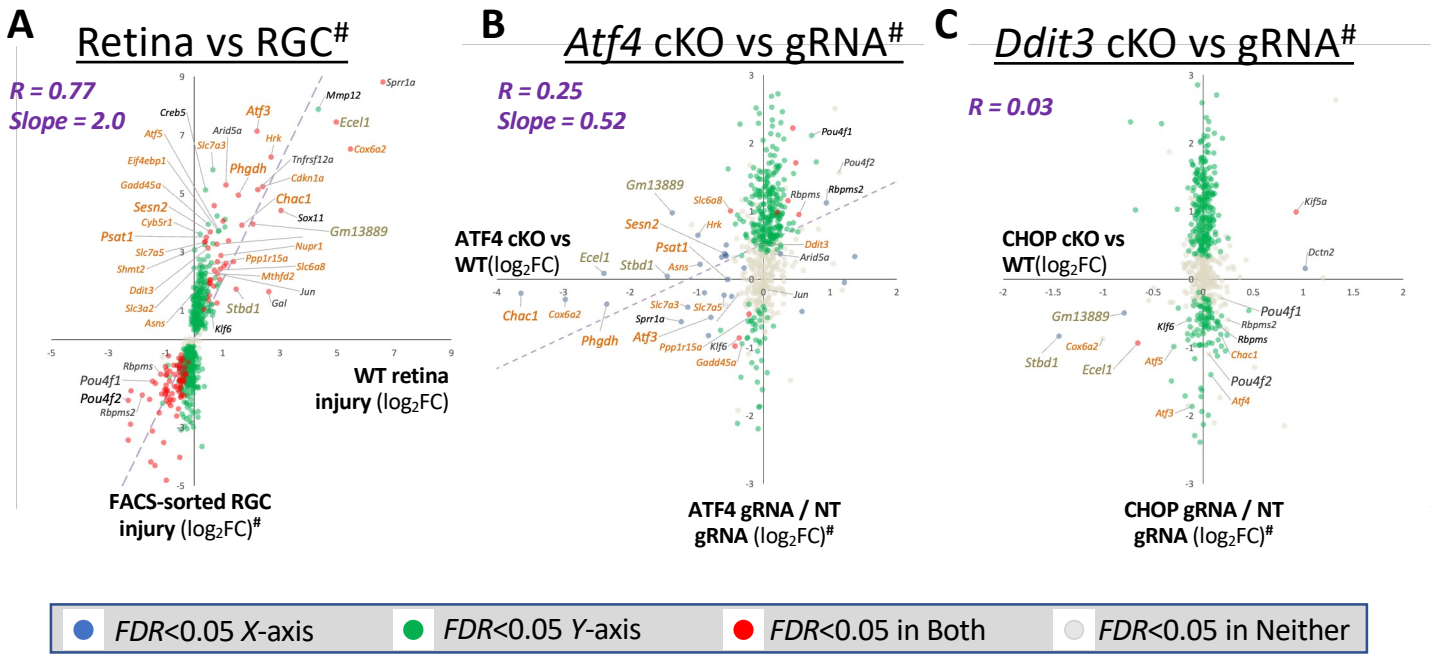
A
Retina vs RGC#
R = 0.77
Slope = 2.0
WT retina injury (log2FC)
FACS-sorted RGC injury (log2FC)#
B
Atf4 cKO vs gRNA#
R = 0.25
Slope = 0.52
ATF4 cKO vs WT(log2FC)
ATF4 gRNA / NT gRNA (log2FC)#
C
Ddit3 cKO vs gRNA#
R = 0.03
CHOP cKO vs WT(log2FC)
CHOP gRNA / NT gRNA (log2FC)#
FDR<0.05 X-axis
FDR<0.05 Y-axis
FDR<0.05 in Both
FDR<0.05 in Neither